Am J Stem Cells 2022;11(1):12-27
www.AJSC.us /ISSN:2160-4150/AJSC0136185

Original Article

Defects in energy metabolism are associated with functional exhaustion of bone marrow mesenchymal stem cells in cirrhosis

Dhananjay Kumar[1], Deepanshu Maheshwari[1], Nidhi Nautiyal[1], Smriti Shubham[1], Sheetalnath Rooge[1], Lovkesh Anand[2], Ashish Vyas[1], Rekha Kumari[1], Shvetank Sharma[1], Chhagan Bihari[3], Sujata Mohanty[4], Rakhi Maiwall[2], Anupam Kumar[1], Shiv Kumar Sarin[2]

[1]Department of Molecular and Cellular Medicine, Institute of Liver and Biliary Sciences, New Delhi, India; [2]Department of Hepatology, Institute of Liver and Biliary Sciences, New Delhi, India; [3]Department of Pathology, Institute of Liver and Biliary Sciences, New Delhi, India; [4]Stem Cell Facility, All India Institute of Medical Sciences, New Delhi, India

Received June 9, 2021; Accepted January 20, 2022; Epub February 15, 2022; Published February 28, 2022

Abstract: Objectives: Cellular and functional exhaustion of bone marrow mesenchymal stem cells (BM-MSC) is significantly associated with the loss of HSCs and hepatic osteodystrophy in cirrhosis. The molecular mechanisms underlying the dysfunction of BM-MSCs are not well understood. We investigated the underlying mechanisms of cellular and functional exhaustion of BM-MSCs in cirrhosis. Methods: The MSCs were isolated retrospectively from bone marrow of decompensated alcoholic cirrhosis patients {(Trial registration: ClinicalTrials.gov NCT01902511) (n=10; MELD=16.2±2.3; CTP=8.7±2.3)} and age and gender-matched healthy controls (n=8). Global gene expression profile of healthy bone marrow MSCs (hBM-MSCs) and cirrhosis patients BM-MSCs (cBM-MSCs) were done by mRNA sequencing. XFe24-bioanalyzer analyzed the bioenergetic potential of cells. Level of different cytokines and growth factors in BM-plasma and MSCs secretome were analyzed by Luminex-based bead array. Results: Analysis of differentially expressed genes showed significant (P<0.01) up-regulation of genes associated with ubiquitination and catabolism of proteins; TNF signaling, insulin resistance, and down-regulation of genes associated with DNA repair, protein processing, cell cycle, and mitochondrial respiration in cBM-MSCs in comparison to hBM-MSCs. Compared to hBM-MSCs, cBM-MSCs showed a significant defect in glycolysis due to insulin resistance and poor glucose uptake (P=0.002). This led to compromised self-renewal capacity and cellular loss of MSCs in cirrhosis. cBM-MSCs also showed a significant impairment in Oxidative phosphorylation (OXPHOS) due to mitochondrial dysfunction leading to defects in the osteogenic differentiation with early aging and senescence. Conclusion: Compromised energy metabolism due to inflammatory and metabolic stress-induced insulin resistance underlies the cellular and functional exhaustion of BM-MSCs in cirrhosis.

Keywords: Oxidative phosphorylation, glycolysis, bone marrow mesenchymal stem cells, liver cirrhosis

Introduction

Bone marrow (BM) is a reservoir for immune and hematopoietic cells and is critical for tissue repair and regeneration. Patients with liver cirrhosis showed a significant dysfunction of hematopoietic [1, 2] and immune systems (called cirrhosis-associated immune dysfunction syndrome) that compromise the native liver regeneration and increase the risk of infection in these patients [3, 4]. Earlier we showed that derangement of the hematopoietic niche and loss of hematopoietic stem cell (HSCs) reserve contribute to the hematological and immunological dysfunctions and are associated with reduced potential for regeneration in cirrhosis [5].

Bone marrow mesenchymal stem cells (BM-MSCs) [6, 7] or skeletal stem cell [8] are the multipotent bone marrow stromal cells (BMSC) that plays a vital role in the organization of the hematopoietic niche in bone marrow [9-11] and serve as a self-renewing progenitor of skeletal

tissues [9]. Recently we have shown that cellular and functional exhaustion of Nestin+ BM-MSCs are significantly associated with the loss of HSCs [5] and hepatic osteodystrophy [12] in cirrhosis. Apart from physiological role of MSCs as skeletal stem cells and organizers of the hematopoietic niche, they also played an essential role in establishing a regenerative microenvironment in response to injury by secreting bioactive molecules and regulating the local immune response [13]. Due to this remarkable natural healing property these cells have recently received much attention as cells of choice to treat a wide variety of inflammatory clinical pathologies, including liver diseases [14-18]. Despite the promising therapeutic benefit of MSC therapy in an animal model of cirrhosis, the use of autologous BM-MSCs in cirrhotic has shown limited effect [19, 20]. In most of the clinical studies with autologous bone marrow mesenchymal stem cells showed some improvement in Child-Pugh and MELD scores, but they failed to show the distinct clinical benefits [19-21].

Similarly, the histological evidence of improvement in fibro-inflammatory reactions or native liver regeneration remains lacking [14, 20]. Recently in phase 2 clinical study, Suk KT et al. [22] showed autologous BM-MSC transplantation safely improved histologic fibrosis and liver function in patients with compensated alcoholic cirrhosis. While in decompensated cirrhosis, Mohamadnejad M et al. [23] has shown no beneficial effect of autologous bone marrow MSC transplantation through a peripheral vein. This further highlights the functional incapability of BM-MSCs in advance cirrhosis.

Cirrhosis is a state of chronically altered metabolic, inflammatory, and circulatory milieu that will likely adversely affect the BM-MSCs [24]. In the current study, we aim to identify the underlying cause of functional exhaustion of BM-MSCs in cirrhotics.

Methodology

Patients

The retrospective study was conducted on decompensated cirrhosis (DC; n=10) patients, admitted at the Institute of Liver and Biliary Sciences, New Delhi, between July 2013 and October 2014 in which bone marrow examination was done as a part of a clinical study (Trial registration: ClinicalTrials.gov NCT01902511). Inclusion criteria: DC patients with alcohol (abstinence of at least three months) and cryptogenic cirrhosis between 18- and 65-years were included. Exclusion criteria: (a) patients with active sepsis; (b) variceal bleeding; (c) hepatocellular carcinoma (HCC); (d) acute kidney injury (AKI) with serum Creatinine >1.5 mg/dl; (e) multi-organ failure; (f) viral etiology; (g) comorbid diseases; (h) pregnant and (i) those who not given the informed consent were excluded from this study. Leftover bone marrow aspirate after hematopoietic stem cell enumeration were taken for isolation of mesenchymal stem cells.

MSC isolation and cell culture

Fresh bone marrow aspirate of cirrhotic patients (n=10; MELD=16.2±2.3; CTP=8.7±2.3) were obtained with written informed consent using the guidelines approved by the Institutional Committee for Stem Cell Research and Therapy (ICSCRT) and the Institutional Ethics Committee (IEC) at Institute of Liver and Biliary Sciences, New Delhi. MSCs were isolated by using ROSETTESEP™ MSCs enrichment kit from Stem cell technology as per manufacturer protocol. Briefly, 1 ml bone marrow was incubated with RosetteSep™ Enrichment Cocktail (50 µl/ml) for 20 minutes at 25°C. After incubation samples were diluted with PBS containing 2% FBS and 1 nM EDTA (/mL) and centrifuged in a density gradient. Enriched cells from the density gradient medium: plasma interface was removed and washed once in dilution media and resuspended in MesenCult™ MSCs culture media from Stem cell technology. Resuspended cells were plated on tissue culture flask and incubated at 37°C in a CO_2 incubator. For sub-culturing, TryplE Select 10X (Gibco, cat. no. A12177-01) was used. Age and sex-matched healthy Bone marrow MSCs were taken from Dr. Sujata Mohanti's lab and cultured in the same condition. Cells from passage 3 to 5 were used for further experimental analysis.

Phenotypic characterization of MSC

To screen for the presence of MSC positive and negative markers, cells at Passage three were subjected to flow cytometry analysis. The samples were incubated with the following mentioned antibodies for half an hour at room temperature, following which the samples were

analyzed using the FACS. The expression levels of positive markers CD105; CD73; CD90 and negative markers CD34, CD45, and CD14 were analyzed.

In-vitro differentiation to osteo- and adipo-lineage

Adipogenic differentiation was initiated in confluent cultures of MSCs using a complete medium supplemented with 200 mM indomethacin, 0.5 mM 3-isobutyl-1-methylxanthine, 10 mg/ml insulin and 1 mM dexamethasone (all reagents from Sigma-Aldrich). After 18 days, adipogenic differentiation was detected by staining the lipid droplets with Oil Red O (Sigma-Aldrich). Osteogenic differentiation was induced in confluent cultures of MSCs using a complete medium supplemented with 0.1 mM dexamethasone, 10 mM beta-glycerophosphate, and 0.2 mM ascorbic acid (all reagents from Sigma-Aldrich).

Colony-forming unit-fibroblast assay

To assess colony-forming assay equal number (10,000) of healthy and cirrhotic BM-MSCs were plated in 35 mm. The cells were incubated for eight days in MSCs culture media, at which point they were fixed and stained with 0.1% toluidine blue in 1% paraformaldehyde (all reagents from Sigma-Aldrich, St. Louis, MO, USA) to visualize the colonies. Stained colonies were manually counted. The assay for each sample was carried out in triplicate. To access the effect of glycolysis on the colony-forming ability of MSCs, healthy BM-MSCs were cultured in the presence or absence of 2-deoxy glucose (2DG, glycolysis inhibitor; 100 mM).

RNA isolation and transcriptomics analysis

Total cellular RNA was isolated from cBM-MSCs (n=6) and hBM-MSCs (n=6) using the RNeasy mini kit (Qiagen, Venlo, Limburg, Netherlands). According to the manufacturer's instructions, the RNA samples were treated with DNA-free DNase I (Ambion, Life Technologies - Carlsbad, CA, USA), according to the manufacturer's instructions. RNA sequencing was performed using the Illumina Hi-Seq sequencing system at 50 bp read length, and data were deposited to the NCBI database (https://www.ncbi.nlm.nih.gov/sra/PRJNA556-702). FASTQ-formatted sequencing data were de-multiplexed to assign reads to the originating sample. Reads were mapped to the human genome reference (UCSC hg19) using TopHat v2.0.13. Each transcript's total mapped read numbers were determined and normalized to detect fragments per kilobase of exon per million fragments mapped (FPKMs) using Cufflinks. Genes with more than one zero FPKM values out of the analyzed samples were excluded from filtering potentially significant gene expressions. For differential expression gene (DEG) analysis, the values of log2 (FPKM+1) values were calculated, and then normalized by quantile. Transcripts with fold-change values larger than 2 with a p-value ≤ 0.05 were included in the analysis as DE genes. Functional groups and pathways encompassing the DEGs were identified based on GO and KEGG Pathway analysis using the Database for Annotation, Visualization, and Integrated Discovery (DAVID v.6.8) software. The threshold was set as modified Fisher Exact P-value (EASE score) ≤ 0.05.

Seahorse metabolic analysis

Analysis of the extracellular acidification rate (ECAR) and oxygen consumption rate (OCR) was performed with a Seahorse XF24 Extracellular Flux Analyzer instrument in cBM-MSCs and hBM-MSCs at the same passage (p3) as a measure of lactate production (a surrogate for the glycolytic rate) and OXPHOS respectively. In brief, MSCs were seeded in triplicate at a density of 40×10^4 cells per well and cultured overnight in MSCs culture media (alpha-MEM low glucose with 10% MSC grade fetal bovine serum). Before starting the assay, cells were washed and incubated in Seahorse Assay Medium supplemented with 10 mM glucose and 1 mM sodium pyruvate and glutamine in 37°C incubator without CO_2 for 45 min. Glucose and pyruvate were not added in assay media for the glycolysis stress test. The parameter of oxidative phosphorylation was calculated by a real-time change in OCR in response to treatment with Oligomycin (ATPase inhibitor, 1 μM), FCCP (0.2 μM) and rotenone (0.5 μM). Similarly, change in glycolytic parameters were analyzed by measuring the real-time change in ECAR in response to treatment with glucose (final concentration 10 mM; Sigma Aldrich, St. Louis, MO, USA), oligomycin (final concentration 5 μM; Sigma Aldrich) and 2-deoxy-d-glucose (2DG, final concentration 100 mM; Seahorse Bioscience).

Measurement of mitochondrial contents

To measure the mitochondrial content in passage-3 cBM-MSCs and hBM-MSCs were stained with MitoTracker Green (for total mitochondrial mass) and MitoTracker Red (for mitochondrial membrane potential) according to the manufacturer's protocol (Invitrogen). For flow cytometry analysis, data were acquired with a FACSCalibur flow cytometer (BD Biosciences) and analyzed with FlowJo software (Tree Star).

Measurement of total intracellular ROS, mitochondrial ROS, and glucose uptake

Intracellular ROS levels and mitochondrial ROS levels were analyzed by staining the cells with dihydrorhodamine 123 (Sigma) (for total ROS) and MitoSOX (for mitochondrial ROS). Staining was performed according to the manufacturer's instructions (Invitrogen). After staining, cells were subjected to flow cytometry analysis, and data were acquired with a FACS Caliber flow cytometer (BD Biosciences) and analyzed with FlowJo software (Tree Star). According to the manufacturer's protocol, the glucose uptake capacity of MSCs was measured using 2-NBDG (a fluorescent D-glucose analog)-based Glucose Uptake Assay Kit (Cayman). Fluorescence produced by the cells (glucose uptake capacity) was detected by SpectraMax M5 Microplate Reader (Molecular Devices).

Measurement of cytokines and glucose in BM Plasma

The plasma level of inflammatory cytokines TNF-α, IL6, IL1β, and glucose were analyzed in 25 cirrhotic BM Plasma and ten non-cirrhotic controls. According to the manufacturer's protocols, cytokines were measured by enzyme-linked immunosorbent assay using capture and detection antibodies against TNF-α, IL6, IL1β (eBioscience) according to manufacturer's protocols. Bone marrow plasma levels of glucose were measured by glucose colorimetric assay Kit (Cayman Chemical; Michigan; USA) as per manufacturer's protocols.

Measurement of cell secretome

The conditional medium was harvested from MSC culture in a serum-free medium for 5 hrs. A panel of 39 cytokines, chemokines, and growth factors were measured in cell secretome using a Bio-Plex multiplex cytokine bead assay system (Bio-Rad, CA) as per the manufacturer's protocol. The intra-assay and inter-assay coefficient of variation considered for multiplex assays was <5%.

Senescence assay

Cells grown in Mesen-Cult media were comparatively analyzed for senescent cells in culture at the end of passages 3 and 5. To do so, the cells were cultured up to 60% confluence in 35 mm dishes. According to the manufacturer's protocols, cells were fixed and stained using a Senescence β-Galactosidase Staining Kit (Cell Signaling Technology, Danvers, MA, USA). After overnight incubation with the staining solution, a total of ten 10× pictures per dish were taken under the microscope. Senescent cells were manually counted in each field. The assays were carried out in duplicate.

Determination of MSC proliferation and cell cycle analysis

Cells were seeded in 12-well plates to calculate the population doubling time, and the initial seeding number was determined. Triplicates were then trypsinised and counted after 24, 48, 72 and 96 hours. To analyze the percentage of cells in G1, S, and G2 phases at passage 5, cells were grown in culture media were subjected to propidium iodide (PI) staining. Cultured cells on P5 were harvested, resuspended in Dulbecco's PBS (DPBS) (Invitrogen), and fixed using 70% ethanol. The cells were incubated for 15 minutes on ice. They were then centrifuged and resuspended in 500 µL PI solution in DPBS (50 µg/mL PI), containing 0.1 mg/ml RNase A and 0.05% Triton X-100. The cells were incubated for 40 minutes at 37°C, after which they were centrifuged and resuspended in DPBS for flow analysis.

Statistical analysis

Data are presented as mean ± SD. The statistical significance was calculated using Student's t-test followed by multiple comparison tests using Graph Pad Prism. $P<0.05$ was considered statistically significant.

Study approval

This study was approved by the Institutional Ethics Committee/Review Board (IEC/2017/

49/MA13) and the Institutional Committee for Stem Cell Research and Therapy (ICSCRT) (9/ILBS/IC-SCR/2017) to obtain human bone marrow samples as per the guidelines of Institutional Ethics Committee (IEC) at Institute of Liver and Biliary Sciences, New Delhi, India. Written informed consent was received from participants before inclusion in the study.

Results

All MSCs fulfilled the minimal criteria for mesenchymal stromal cells

Bone marrow mesenchymal stem cells were isolated from decompensated cirrhosis patients (n=10). Age and gender-matched healthy bone marrow MSCs (n=8) were taken as control. Demographic and clinical profiles of patients are summarized in Table S1. The mean age of cirrhotic patients (41.3±5.4 years) and healthy controls (40.25±4.2 years) was comparable. Of the ten cirrhotic patients, seven were alcoholic (with >3 months of abstinence), and three were cryptogenic. The mean MELD (Model for End-Stage Liver Disease) and Child-Turcott-Pugh (CTP) scores of cirrhotic patients were 16.2±2.3 and 8.7±2.3, respectively. Isolated and cultured bone marrow MSC from both cirrhotic patients (cBM-MSCs) and healthy controls (hBM-MSCs) showed characteristic spindle-shaped morphology (Figure S1A) with >90% positivity for surface marker proteins; CD73, CD105, CD90 and <2% positivity for CD45, CD14, and CD34 (Figure S1B). In response to osteo- and adipose-differentiation media, while cBM-MSCs and hBM-MSCs showed *in-vitro* osteo- and adipose-differentiation respectively (Figure S1C), the number of oil red "O" positive adipocytes was higher (P<0.001) in cBM-MSCs in comparison to hBM-MSCs (Figure S1D). Together these data showed that both normal and diseased MSCs fulfilled the minimal criteria for mesenchymal stromal cells as described [25].

Cirrhotic BM-MSCs show increased inflammatory and metabolic stress

Recently we showed the cellular, and functional exhaustion of Nestin+ BM-MSCs is significantly associated with the loss of HSCs [5] and hepatic osteodystrophy [12] in cirrhosis. To further understand the underlying cause of this functional exhaustion in cirrhotic BM-MSCs, we analyzed the transcriptomes of cirrhotic and healthy bone marrow MSCs. RNA sequencing identified 19,382 protein-coding genes (https://www.ncbi.nlm.nih.gov/sra/PRJNA556-702). At the threshold set to "P<0.05, (fold change) FC>2", 5234 gens were found to be differentially expressed between cirrhotic and healthy bone marrow MSCs of which 4360 were upregulated and 869 were down-regulated in cBM-MSCs in comparison to hBM-MSCs (Table S2). Next, we categorized these differentially expressed genes into enriched categories (Biological Process, Cellular Component, and Molecular Function) according to GO analysis (details summarized in **Figure 1A**, **1B**; Tables S3, S4). Further annotation by KEGG pathway analysis showed genes up-regulated in cBM-MSCs were significantly (P<0.01) linked to VEGF-signaling, platelet activation, mTOR signaling, TNF signaling, insulin resistance, amino and nucleotide sugar metabolism and cellular senescence (**Figure 1A**; Table S3), genes down-regulated were significantly linked to DNA repair, glutathione metabolism, oxidative phosphorylation, cell cycle, AMPK signaling, transcription and protein processing in the endoplasmic reticulum (**Figure 1B**; Table S4).

Insulin resistance compromise glycolysis in Cirrhotic BM-MSCs

Our RNA-Seq data showed a significant increase in genes associated with insulin resistance in cirrhotic BM-MSCs. This can adversely affect the glycolysis, which is required to maintain the stemness of MSCs [26, 27]. Hence, we next analyzed the glycolytic potential of cBM-MSCs and hBM-MSCs by studying the changes in extracellular acidification rate (ECAR) in response to glucose, oligomycin (OM), and 2-deoxyglucose (2-DG) injection. We found in comparison to hBM-MSCs, the cBM-MSCs showed a significant decrease in both glycolysis (P<0.001) and glycolytic reserve (P<0.001) (**Figure 2A**). However, our RNA-seq data showed a significant increase in the expression of genes encoding enzymes in the glycolytic pathway *Hk1, pfkp, Eno2, Aldoc* (Figure S2), the cBM-MSCs showed a significantly (P=0.002) compromised glucose uptake capacity (**Figure 2B**). In comparison to hBM-MSCs, cBM-MSCs also showed significant (P=0.0004) decrease in their colony-forming unit-fibroblast (CFU-F) capacity, indicating compromised self-renewal

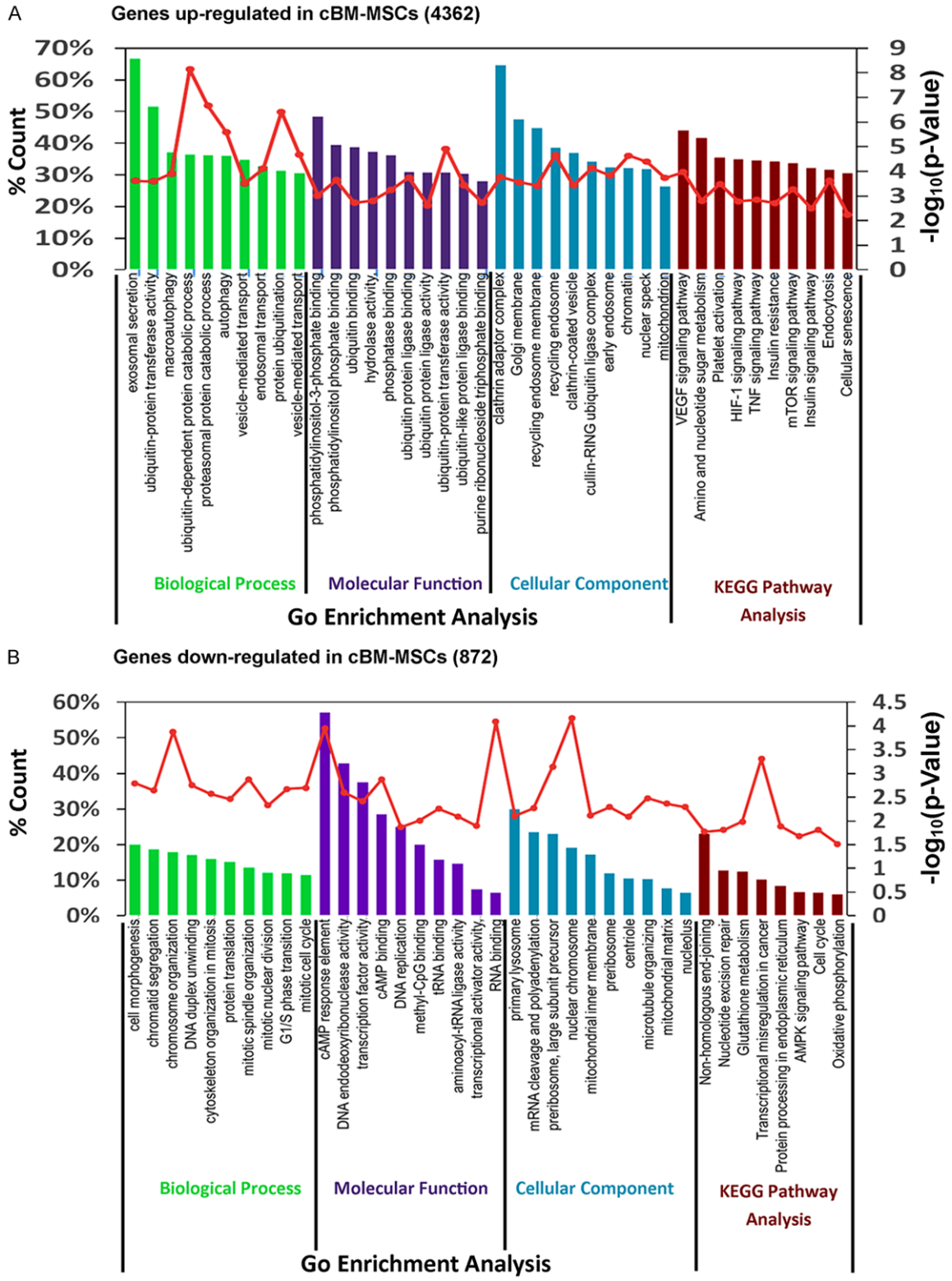

Figure 1. GO-enrichment and KEGG-pathway analysis of differentially expressed genes between healthy and cirrhotic human BM-MSCs. A. Graph showing GO-enrichment and KEGG-pathway analysis of genes significantly upregulated in cBM-MSCs in comparison to hBM-MSCs. B. Graph showing GO-enrichment and KEGG-pathway analysis of genes significantly downregulated in cBM-MSCs in comparison to hBM-MSCs. Note: The bar chart represents % of genes count, and the red dot represents the -$\log_{10}$ (*P*-value).

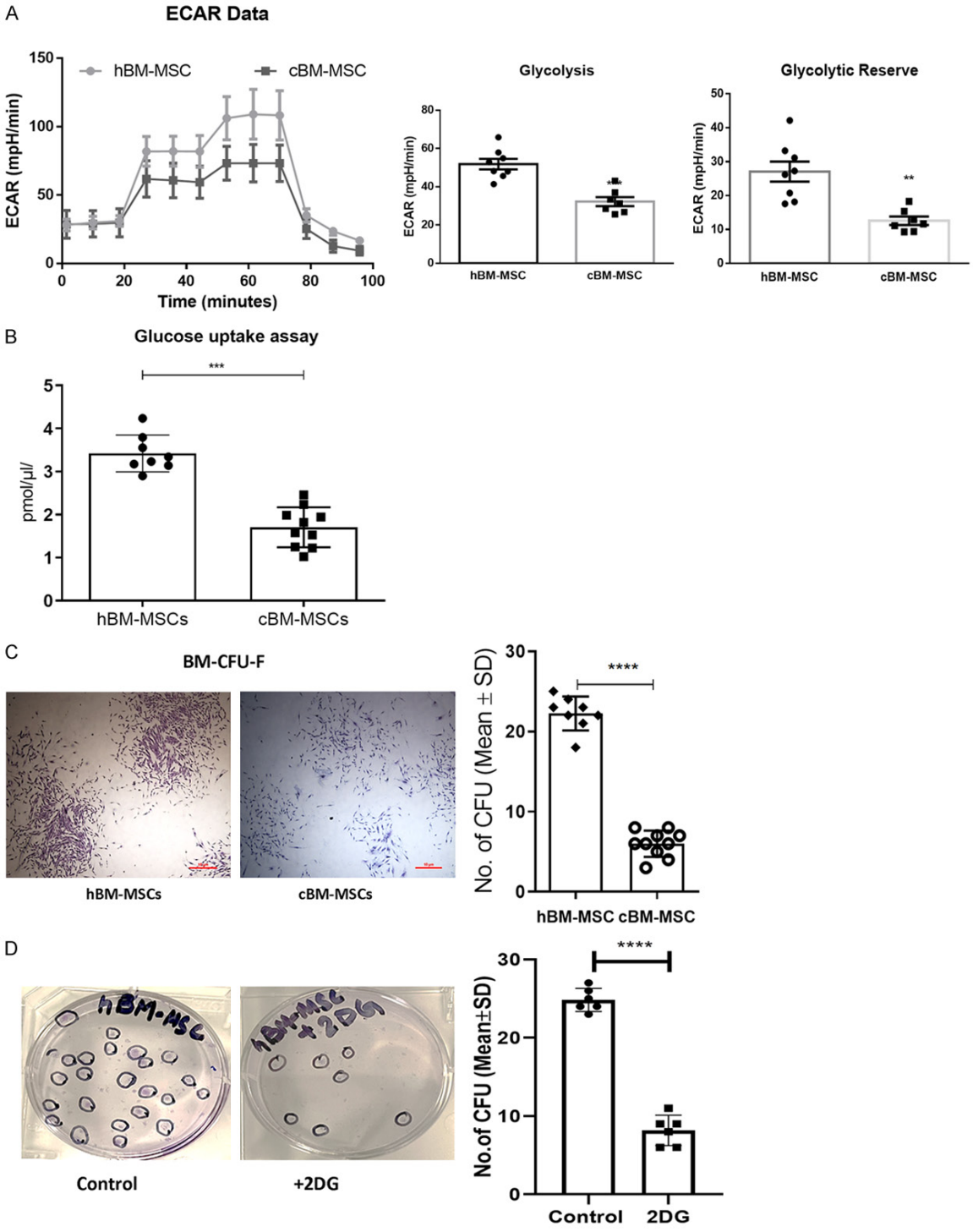

Figure 2. Measurement of glycolytic potential and CFU-F of healthy and cirrhotic BM-MSCs: (A) (left) Graph showing the real-time change in ECAR in response to glucose, oligomycin, and 2-deoxyglucose (2DG) to determine glycolysis parameters in healthy and cirrhotic BM-MSCs (right) graph showing glycolysis and glycolytic reserve in healthy and cirrhotic BM-MSCs. (B) Bar-graph showing glucose uptake (2-DG6P pmol/µl) in healthy and cirrhotic BM-MSCs. (C) Individual colonies captured at 4× magnification, for hBM-MSC and cBM-MSCs (left) and Bar graph (right) showing an average number of CFU-F colonies (Mean ± SD) generated per 1000 cells at passage three by hBM-MSC and dBM-MSCs. (D) Graph showing an average number of CFU-F colonies (Mean ± SD) of healthy BM-MSCs with and without 2DG (glycolysis inhibitor). **<0.005; ***<0.0005; ****<0.0001.

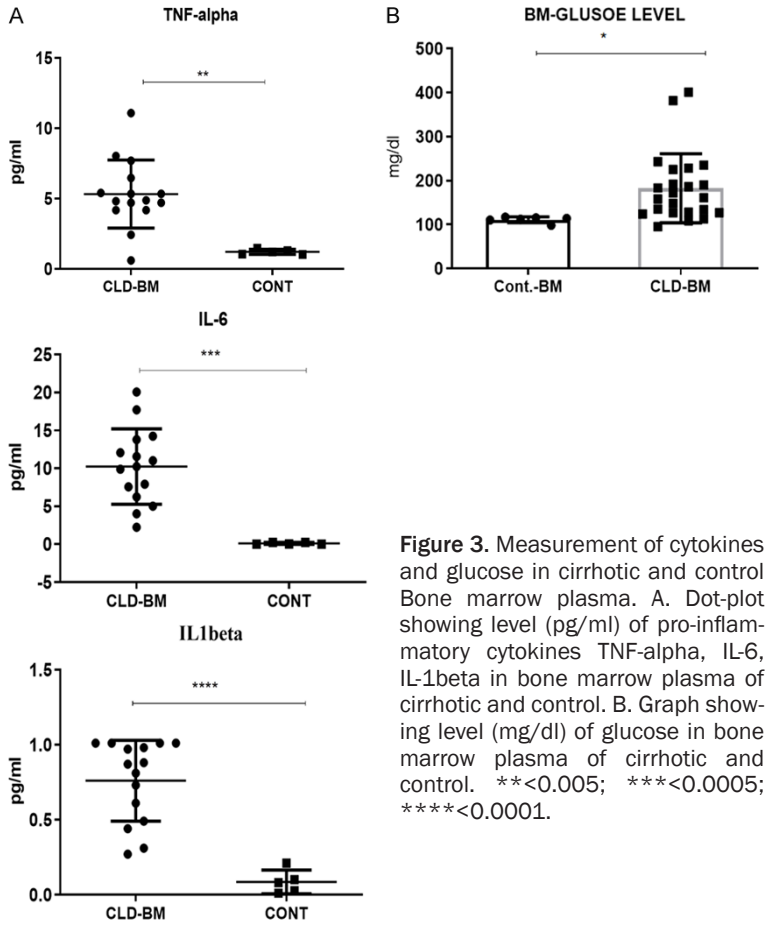

Figure 3. Measurement of cytokines and glucose in cirrhotic and control Bone marrow plasma. A. Dot-plot showing level (pg/ml) of pro-inflammatory cytokines TNF-alpha, IL-6, IL-1beta in bone marrow plasma of cirrhotic and control. B. Graph showing level (mg/dl) of glucose in bone marrow plasma of cirrhotic and control. **<0.005; ***<0.0005; ****<0.0001.

potential of cBM-MSCs (**Figure 2C**). As MSCs rely on glycolysis to meet their energy demand, to further confirm whether defect in glycolysis is associated with poor self-renewal capacity of cBM-MSCs, we analyze the CFU-F ability of hBM-MSCs in the presence or absence of glycolysis inhibitor (2-deoxy-D-glucose, 2-DG). In comparison to control, hBM-MSCs treated with 2-DG showed a significant (P<0.0001) decreased number of CFU-F (**Figure 2D**), suggesting glycolysis is essential to maintain the stemness of MSCs.

cBM-MSCs also showed a significant increase in genes associated with TNF-α signaling (**Figure 1A**) and various inflammatory cytokines have been shown to induce insulin resistance [28]. Hence, we further analyze the level of inflammatory cytokines in the BM-plasma of cirrhotic and healthy control. In comparison to healthy BM-plasma, cirrhotic bone marrow plasma showed a significant increase in the level of inflammatory cytokines; TNF-α (P= 0015), IL-6 (0.0003) IL1β (P< 0.0001) (**Figure 3A**). Cirrhotic BM-Plasma also showed a significant increase in glucose level (P=0.0369) in comparison to healthy BM plasma (**Figure 3B**). Together, these data suggested that increased inflammatory cytokines (TNF-α, IL1β, IL6) and hyperglycemia in cirrhotic BM environment may induce insulin resistance (Figure S3) and glycolysis dysfunction that leading to the loss of self-renewal capacity of BM-MSCs in cirrhotic.

Cirrhotic BM-MSCs show compromised OXPHOS and mitochondrial dysfunction

As cirrhotic BM-MSCs showed a defect in glycolysis, we studied their OXPHOS potential. We assessed the functional profile of mitochondria (**Figure 4A**). In comparison to hBM-MSCs, cBM-MSCs showed a significant decrease in both basal (P<0.01), maximum (P< 0.01), and ATP linked (P<0.01) (**Figure 4B**) respiration. Our RNA-Seq data showed a significant decrease in expression of genes associated with OXPHOS (*PPA1, NDUFA3, ATP6A2, COX11, NDUFB1, COX7C, LHPP, COX6B1*) in cBM-MSCs in comparison to hBM-MSCs (Table S4). The cBM-MSCs also showed a significant (P<0.01) decrease in Proton leak in comparison hBM-MSCs (**Figure 4C**). However, both mitochondrial (P<0.01) and total (P<0.001) ROS levels were significantly high in cBM-MSCs in comparison to hBM-MSCs (**Figure 4D**). This can lead to the increased mitochondrial damage [29]. Next, to investigate whether the loss of mitochondrial respiration in cBM-MSCs resulted from the loss of mitochondrial mass or accumulation of dysfunctional mitochondria, we stained the cells with MitoTracker Green (MTG) for total mitochondrial content, regardless of mitochondrial membrane potential (ΔΨm) and found that cBM-MSCs had a slightly high mitochondrial mass in comparison to hBM-MSCs (**Figure 4E**), however, it was stati-

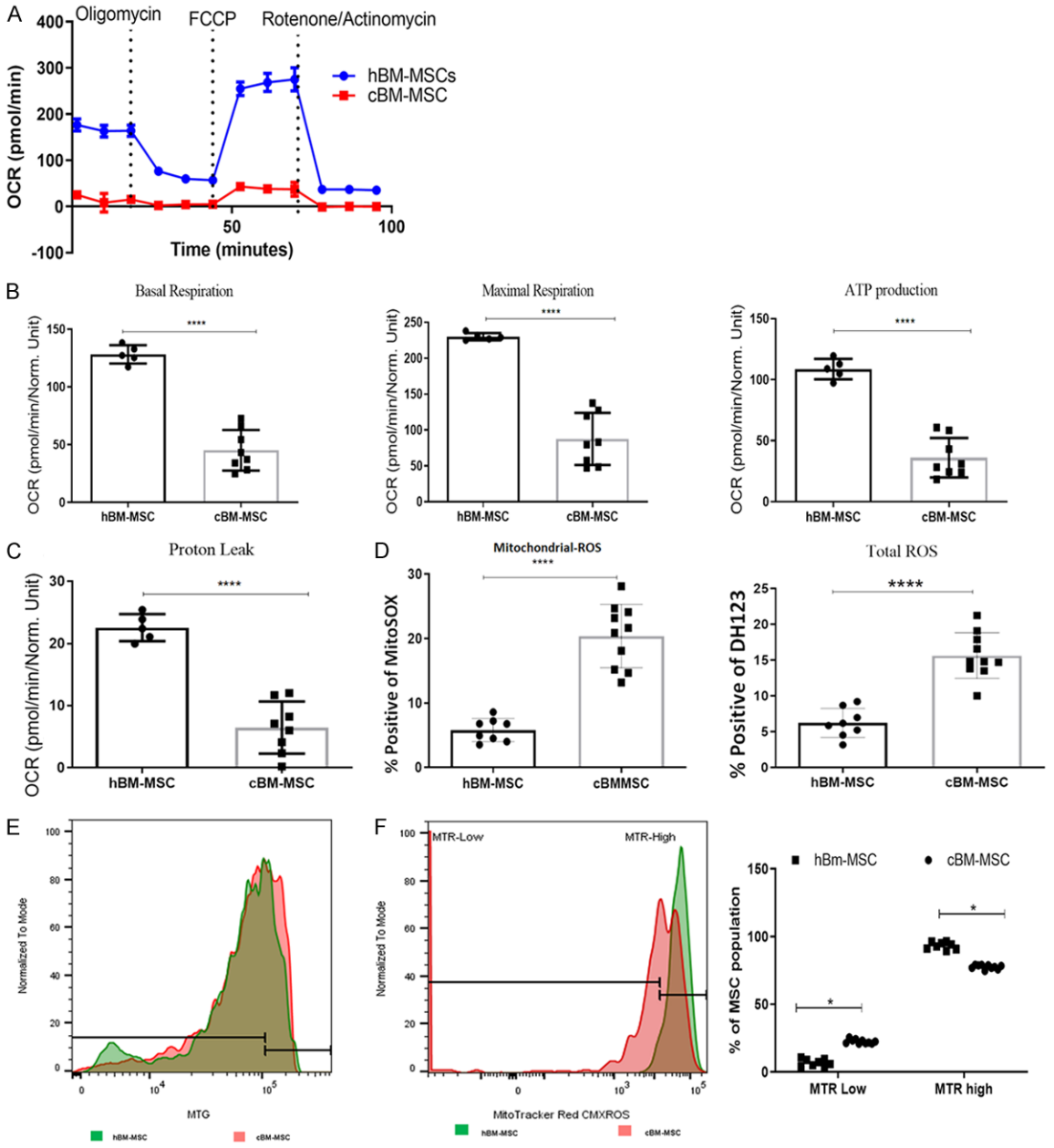

Figure 4. Measurement of mitochondrial function and content in healthy and cirrhotic BM-MSCs. A. Graph showing a real-time change in OCR in response to oligomycin, FCCP, and Rotenone/Antimycin to determine mitochondrial respiration parameters in healthy and cirrhotic BM-MSCs. B. Bar-graph showing mitochondrial respiration as a measure of OCR linked to baseline respiration, Maximal reparation, ATP linked respiration in healthy and cirrhotic BM-MSCs. C. Bar-graph showing Proton leak linked respiration in healthy and cirrhotic BM-MSCs. D. Bar-Graph showing mitochondrial and total ROS levels in healthy and cirrhotic BM-MSCs. E. A Representative image showing total mitochondrial mass in healthy and cirrhotic BM-MSCs. F. Graph showing functional mitochondrial mass in healthy and cirrhotic BM-MSCs. ****P<0.0001.

cally not significant. Further to access the proportion of functional mitochondrial mass, we used MitoTracker Red (MTR, ΔΨm-dependent mitochondrial stain) to distinguish between respiring mitochondria and dysfunctional mitochondria [30]. In comparison to hBM-MSCs cirrhotic BM-MSCs showed a significant (P<0.01) decrease in functional mitochondria (MTR+) (**Figure 4F**). Combined, our data revealed that loss of functional mitochondrial mass leads to

a gross defect in mitochondrial energy metabolism in cBM-MSCs.

Cirrhotic BM-MSCs shows early senescence and functional exhaustion

While glycolysis is required to maintain the stemness and preserve the long-term self-renewal potential of MSCs [26, 27], OXPHOS drive their differentiation to osteoblast [31] as well as their immunomodulatory function [32, 33]. As we observed significant impairment of OXPHOS in cBM-MSCs, we next compare the osteogenic differentiation and immunomodulatory function of cirrhotic and healthy BM-MSCs. To analyze the osteogenesis potential, we measure the relative expression of various osteogenesis associated marker gene expressions in *in-vitro* osteo-differentiated hBM-MSCs and cBM-MSCs. RT-PCR analysis showed >2-fold decrease in expression of osteogenic marker genes; *Osteocalcin, COL1, ALP and Runex2* in cBM-MSCs in comparison to hBM-MSCs (**Figure 5A**) which is consistent with our previous report [12]. Immunomodulatory properties of MSCs were analyzed by studying the effect of MSCs on T-cell proliferation. In co-culture with anti-CD3 and anti-CD28 induced T cell activated peripheral blood mononuclear cells (PBMCs). At the same time, hBM-MSCs significantly decreased the percentage of activated CD4 (P<0.004) and CD8 (P<0.004) T-cells in comparison to activated T cells alone, cBM-MSCs failed to suppress the CD3/CD28 induced proliferation of CD4 and CD8 T-cells (**Figure 5B**).

Most of the immune regulatory and regenerative functions of MSCs are performed by the various trophic and paracrine factors produced by these cells. To study the paracrine functions, we analyzed a panel of 39 different cytokines/chemokines and growth factors in conditioned media of both healthy and cirrhotic BM-MSCs. Thirty-six (92%) of 39 growth factors, cytokines, and chemokines analyzed were found to be downregulated in cBM-MSCs secretome in comparison to hBM-MSCs. The cBM-MSCs showed a significant (>2 fold) decrease in the level of EGF, GM-CSF, FGF-1, TWEAK, IFN-G, IL12, IL15, IL17, IL9, IL1B, Il6, Il8, IP10, MCP1, MIP1A, MIP1B, TNFA, TNFB, IL10, il13, IL1RA, IL2, IL4, IL7 and an increase in RANTES and TGF-A (**Figure 5C**), suggesting defective paracrine function of cBM-MSC.

Mitochondrial dysfunction is associated with senescence and aging in various cells [34, 35] and our RNA-seq data showed significant increase in genes associated with cellular senescence (**Figure 2A**) and decreased genes associated with the cell cycle. To further understand the aging-associated changes, we compared population doubling time and senescence-associated-beta-galactosidase (SA-beta-gal) positivity of both cirrhotic and healthy BM-MSCs. At P3, the average population doubling time of hBM-MSCs was 25.9±1.35 hours, and cBM-MSCs were 47.3±3.8 hours, which was significantly higher in cBM-MSCs (P< 0.001). At P5, though hBM-MSCs (29.19± 1.78) did not show much change in population doubling time, this was significantly (P<0.0001) increased in cBM-MSCs to 75.72±4.59 (**Figure 5D**). Further, cell cycle analysis of both hBM-MSCs and cBM-MSCs at P5 showed a significant increase in G1 (P=0.0079) and decrease in S (P=0.0073) and G2 (P=0.0068) phases of cells in comparison to hBM-MSCs (Figure S4), suggesting an early loss of replicative potential of cBM-MSCs due to G1 arrest. SA-beta-gal staining also showed significant differences in the number of SA-beta gal positive cells between the hBM-MSCs and cBM-MSCs at both passage 3 (P=0.0004) and passage 5 (P=0.0004). While the average SA-beta gal positive cells in hBM-MSCs remained 1.5±0.89 (passage 3) and 2.25±0.68 (passage 5), in cBM-MSCs, the number of senescent cells progressively increased from 26.9±2.91 (P3) to 57.2±4.62 (**Figure 5E**). Combined, these data suggested the potential link between mitochondrial dysfunction, early senescence/aging and functional exhaustion of cBM-MSCs.

Discussion

This study showed that broad defects in energy metabolism underlie the cellular and functional exhaustion of bone marrow mesenchymal stem cells in cirrhotics. Our data showed that increased inflammatory and metabolic stress in the bone marrow milieu induces insulin resistance and glycolytic dysfunction in cirrhotic bone marrow MSCs, resulting in loss of their self-renewal capacity. Cirrhotic bone marrow MSCs were also defective in their mitochondrial respiration required for their osteogenic and immunomodulatory function.

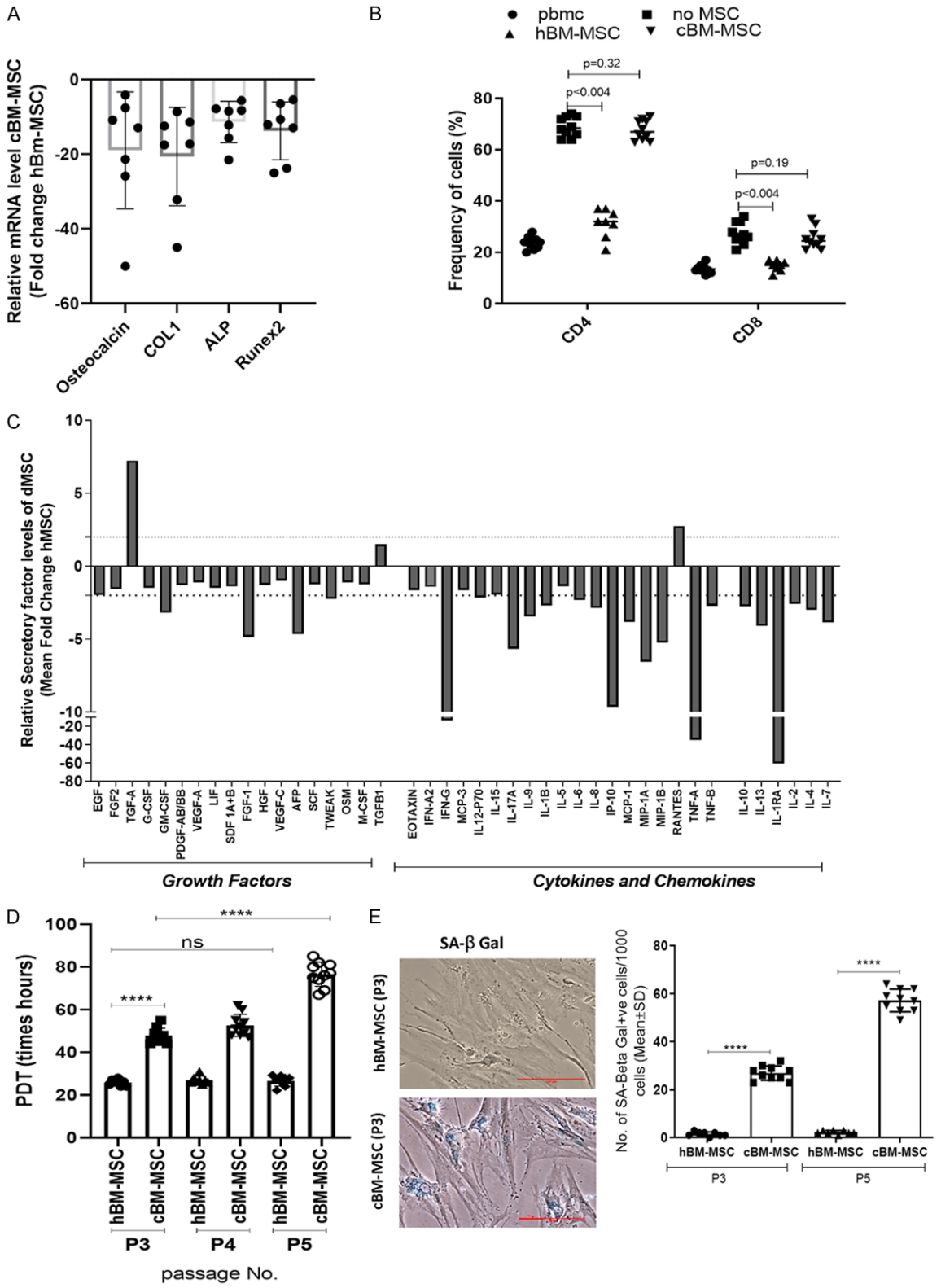

Figure 5. Assessment osteogenic and immunomodulatory function and senescence associated change in in healthy and cirrhotic BM-MSCs. A. Graph showing relative mRNA level of indicated osteogenic marker gene expression in *in-vitro* osteo-differentiated cBM-MSCs in comparison to hBM-MSCs. B. Bar graph showing the percentage of CD4 and CD8-T cells in CD3/CD28 induced T cell activated PBMCs culture alone or in the presence of hBM-MSCs or cBM-MSCs. C. Bar graph showing relative level of indicated cytokines and growth factors secreted in the culture

medium of cBM-MSC with respect to hBM-MSC. D. Bar graph showing population doubling time (in hours) at P3, P4 and P5 of hBM-MSC and cBM-MSCs (*P<0.01). E. Representative picture showing SA-Beta Gal positive cells at passage three culture of hBM-MSCs and cBM-MSCs (Left) and Bar graph (right) showing number of SA-Beta Gal positive cells/1000 of cells (mean ± SD) at P3 and P5 culture of healthy and cirrhotic BM-MSCs (Magnification 40×).

Patients with liver cirrhosis showed a significant defect in hematopoiesis [1, 2] and bone loss in the form of osteopenia and osteoporosis [36]. BM-MSCs play a vital role in the organization of the hematopoietic niche in bone marrow [9-11] and serve as a self-renewing progenitor of skeletal tissues [9]. Earlier, we have shown that cellular and functional exhaustion of Nestin+ BM-MSCs are associated with loss of HSCs [5] and hepatic osteodystrophy [12] in cirrhosis. Underlying cause of observed cellular and functional defect in cirrhotic bone marrow MSCs are not defined. In the global transcriptome profile of cirrhotic and healthy bone marrow MSCs, we observed significant up-regulation of genes associated with TNF signaling, insulin resistance, amino and nucleotide sugar metabolism and cellular senescence and down-regulation of genes associated with DNA repair, glutathione metabolism, oxidative phosphorylation, cell cycle, AMPK signaling, transcription and protein processing in the endoplasmic reticulum in cBM-MSCs compare to hBM-MSCs. Together this suggests an increased in inflammatory and metabolic stress and compromised DNA repair, protein processing, cell cycle, and mitochondrial respiration in cirrhotic BM-MSCs.

Interestingly our RNA-Seq data showed significant increase in genes associated with insulin resistance in cirrhotic BM-MSCs (**Figure 1A**). They showed significantly compromised glucose uptake capacity compared to hBM-BMSCs (**Figure 2B**). This suggests insulin resistance and defect in glucose metabolism in cBM-MSCs. Persistent chronic inflammation with progressive loss in the hepatic reserve has increased the systemic inflammatory, metabolic and oxidative stress in cirrhosis [3, 37]. cBM-MSCs also showed a significant increase in genes associated with TNFα signaling (**Figure 1A**) and various inflammatory cytokines have been shown to induce insulin resistance [28]. Indeed we observed that cirrhotic patients' bone marrow milieu is hyperglycemic (**Figure 3B**) and has significantly increased the level of inflammatory cytokines TNF-α, IL-6, IL-1β in comparison to healthy (**Figure 3A**). These data indicate that increased inflammatory and metabolic stress in cirrhotic bone marrow environments may induce insulin resistance in cBM-MSCs.

Insulin resistance can adversely affect glycolysis. Indeed cirrhotic BM-MSCs showed a significant reduction in both glycolysis and glycolytic reserve (**Figure 2A**) even with the increased expression of several glycolytic genes (Figure S2) compared to hBM-MSCs. This indicates that poor glucose uptake due to insulin resistance compromises the glycolytic potential of cBM-MSCs. In the bone marrow MSCs reside in a hypoxic niche and rely mainly on glycolysis for their energy supply [26] which maintains their long-term self-renewal potential [27]. Compared to hBM-MSCs, cBM-MSCs also showed a significant reduction in their self-renewal capacity (**Figure 2C**). We demonstrated that inhibition of glycolysis in hBM-MSCs significantly reduces their self-renewal capacity (**Figure 2D**). Together these data suggested that defect in glycolysis due to insulin resistance compromises the self-renewal capacity of BM-MSCs in cirrhotics. This also explains the loss of Nestin+ BM-MSCs in cirrhotic bone marrow [5, 12].

While glycolysis is required to maintain the stemness and preserve the long-term self-renewal potential of MSCs [26, 27], OXPHOS drive their differentiation to osteoblast [31] as well as their immunomodulatory function [32, 33]. Our data have shown impairment of mitochondrial respiration in cirrhotic BM-MSCs which fail to compensate for the increased energy demand of cells. Compared to hBM-MSCs, the cBM-MSCs show a significant decrease in basal, maximal, and ATP linked respiration (**Figure 4A**) with decreased expression of various genes (*PPA1, NDUFA3, ATP6A2, COX11, NDUFB1, COX7C, LHPP, COX6B1*) associated with OXPHOS. Emerging evidence has shown that mitochondrial energy metabolism plays a central role in lineage differentiation of MSCs to osteoblast [26, 31, 38-41] and inhibition of mitochondrial respiration suppresses the osteoblastogenesis of MSCs [26, 31].

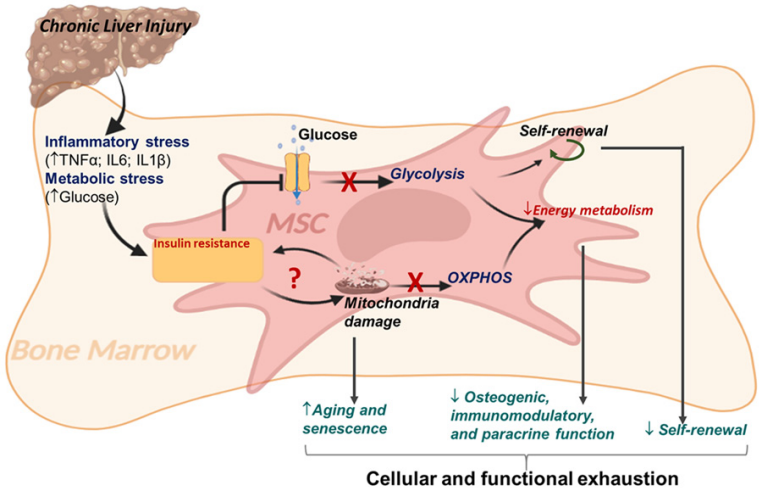

Figure 6. Schematic showing a proposed mechanism of cellular and functional exhaustion of M-MSCs in cirrhosis. Chronic liver injury leads to the accumulation of inflammatory cytokines (TNFα; IL6; IL1β) and hyperglycemia in bone marrow milieu. This induces insulin resistance in cirrhotic BM-MSCs. Poor glucose uptake due to insulin resistance compromises the glycolysis leading to poor self-renewal and loss of MSCs in cirrhotic BM. There is also an accumulation of defective mitochondria leading to a gross defect in mitochondrial respiration that may underline the defect in osteogenic, paracrine, and immunomodulatory function. Mitochondrial damage may also lead to premature aging and senescence in these MSCs. Altogether, broad defect in energy metabolism underlies the cellular and functional exhaustion of BM-MSCs in cirrhotic.

Switch to mitochondrial OXPHOS from glycolysis leads to the activation of canonical Wnt/β-catenin pathway. This leads to the expression of downstream master regulators of osteogenesis, including runt-related transcription factor 2 (Runx2) and Osterix (Osx) [31, 41, 42]. Together with a defect in mitochondrial respiration, cBM-MSCs have also shown impairment of osteogenesis (**Figure 5A**). Hence, the impairment of OXPHOS in cirrhotic BM-MSCs might decrease osteogenesis [12] and bone loss in cirrhotic.

Apart from the physiological role of MSCs as skeletal stem cells and organizer of the hematopoietic niche, they also played an important role in establishing a regenerative microenvironment in response to injury by secreting bioactive molecules and regulating the local immune response [13]. Compared to hBM-MSCs, cBM-MSCs also showed a significant defect in their immunomodulatory (**Figure 5B**) and paracrine (**Figure 5C**) function. Our RNA-seq data shown a significant increase in genes associated with protein catabolism (**Figure 2A**) and decrease in genes associated with transcription and translational machinery (**Figure 2B**) in cBM-MSCs. This may contribute to their compromised paracrine function required for both regenerative and immunoregulatory functions of MSCs. The cBM-MSCs also showed a significant decrease in proton leak (**Figure 4C**) with increased total and mitochondrial ROS (**Figure 4D**). The proton leaks play a critical role in reducing reactive oxygen species (ROS) in cells and protecting the mitochondria from ROS-induced damage [29, 43]. In comparison hBMSc, though total mitochondrial mass slightly increased in cBM-MSCs (**Figure 4E**), they showed a significant reduction of functional mitochondrial mass (**Figure 4F**). This suggests that loss of functional mitochondria is responsible for compromised mitochondrial energy metabolism in cBM-MSCs. Mitochondrial dysfunction has been previously reported in human umbilical cord MSCs of diabetic and obese individuals [44]. Recently, mitochondrial fitness has been associated with the immunomodulatory function of mesenchymal stem cells [32, 33]. Hence, defect in transcription/translational machinery with increased protein catabolism and defect in mitochondrial respiration might contribute to defective loss of immunomodulatory and paracrine function in cirrhotic BM-MSCs. This also provides the possible resign for no beneficial effect of autologous bone marrow MSC transplantation in decompensated cirrhosis [23].

Mitochondrial dysfunction has been associated with cellular senescence and aging [34] and has recently been shown to induce senescence [35]. In our study, we also observed a significant increase in aging-associated changes in cBM-MSCs. Compared to hBM-MSCS, the cBM-MSCs showed replication arrest (**Figure 5D**) and increased senescence-associated SA-β gal positivity (**Figure 5E**) even at early passages. This raises the possible link between insulin resistance, mitochondrial dysfunction, and early senescence, and aging in cBM-MSCs.

In summary, the current study documents the increased inflammatory and metabolic stress in tcirrhosyic patients' bone marrow milieu, inducing insulin resistance in the BM-MSCs. This compromises glycolytic potential, leading to poor self-renewal capacity and cellular loss of MSCs in cirrhotic. Cirrhotic BM-MSCs are not only defective in their glycolysis, but they also showed a gross defect in OXPHOS due to mitochondrial dysfunction, which may underline their early senescence, aging, and functional exhaustion (**Figure 6**). This also explains the poor clinical response of autologous BM-MSCs transplantation in some cirrhosis patients. Hence the therapy (like metabolic regulator drug) targeting the restoration of BM-MSCs bioenergetics might be helpful in the prevention of BM dysfunction as well as osteoporosis in cirrhotic.

Acknowledgements

This work was supported by the Science and Engineering Research Board (SERB), Government of India Grant IR/SB/EF/02/2016. mRNA sequencing was done by DNA Expert Pvt Ltd, Delhi, India.

Disclosure of conflict of interest

None.

Abbreviations

BM-MSC, bone marrow mesenchymal stem cells; HSCs, hematopoietic stem cells; ALD, alcohol-associated liver disease; hBM-MSCs, healthy bone marrow MSCs; cBM-MSCs, cirrhosis patients BM-MSCs; OXPHOS, Oxidative phosphorylation; CTP, Child-Turcott-Pugh; MELD, Model for End-Stage Liver Disease; ECAR, extracellular acidification rate; OM, oligomycin; 2-DG, 2-deoxyglucose; CFU-F, colony-forming unit-fibroblast; FCCP, p-trifluoromethoxyphenyl-hydrazone; ΔΨm, mitochondrial membrane potential; MTR, Mito-Tracker Red; PBMCs, peripheral blood mononuclear cells; SA-beta-gal, senescence-associated-beta-galactosidase; ICSCRT, Institutional Committee for Stem Cell Research and Therapy; FPKMs, fragments per kilobase of exon per million fragments mapped; DEG, differential expression gene; OCR, oxygen consumption rate; PI, propidium iodide; IEC, Institutional Ethics Committee.

Address correspondence to: Dr. Shiv Kumar Sarin, Department of Hepatology, Institute of Liver & Biliary Sciences (ILBS), New Delhi 110070, India. Tel: +91 (011) 46300000; Fax: +91 (011) 26123504; E-mail: shivsarin@gmail.com; Dr. Anupam Kumar, Department of Molecular and Cellular Medicine, Institute of Liver & Biliary Sciences (ILBS), New Delhi 110070, India. Tel: +91 (011) 46300000; Fax: +91 (011) 26123504; E-mail: dr.anupamkumar.ilbs@gmail.com

References

[1] Witters P, Freson K, Verslype C, Peerlinck K, Hoylaerts M, Nevens F, Van Geet C and Cassiman D. Review article: blood platelet number and function in chronic liver disease and cirrhosis. Aliment Pharmacol Ther 2008; 27: 1017-1029.

[2] Sheikh MY, Raoufi R, Atla PR, Riaz M, Oberer C and Moffett MJ. Prevalence of cirrhosis in patients with thrombocytopenia who receive bone marrow biopsy. Saudi J Gastroenterol 2012; 18: 257-262.

[3] Albillos A, Lario M and Alvarez-Mon M. Cirrhosis-associated immune dysfunction: distinctive features and clinical relevance. J Hepatol 2014; 61: 1385-1396.

[4] Arandjelovic S and Ravichandran KS. Phagocytosis of apoptotic cells in homeostasis. Nat Immunol 2015; 16: 907-917.

[5] Bihari C, Anand L, Rooge S, Kumar D, Saxena P, Shubham S, Sukriti, Trehanpati N, Kumar G, Pamecha V, Sharma S, Rastogi A, Kumar A and Sarin SK. Bone marrow stem cells and their niche components are adversely affected in advanced cirrhosis of the liver. Hepatology 2016; 64: 1273-1288.

[6] Caplan AI. Mesenchymal stem cells. J Orthop Res 1991; 9: 641-650.

[7] Pittenger MF, Mackay AM, Beck SC, Jaiswal RK, Douglas R, Mosca JD, Moorman MA, Simonetti DW, Craig S and Marshak DR. Multilineage potential of adult human mesenchymal stem cells. Science 1999; 284: 143-147.

[8] Bianco P and Robey PG. Skeletal stem cells. In: Handbook of Adult and Fetal Stem Cells, Lanza RP. Academic Press; San Diego: 2004. pp. 415-424.

[9] Sacchetti B, Funari A, Michienzi S, Di Cesare S, Piersanti S, Saggio I, Tagliafico E, Ferrari S, Robey PG, Riminucci M and Bianco P. Self-renewing osteoprogenitors in bone marrow sinusoids can organize a hematopoietic microenvironment. Cell 2007; 131: 324-336.

[10] Mendez-Ferrer S, Michurina TV, Ferraro F, Mazloom AR, Macarthur BD, Lira SA, Scadden DT, Ma'ayan A, Enikolopov GN and Frenette PS.

Mesenchymal and haematopoietic stem cells form a unique bone marrow niche. Nature 2010; 466: 829-834.
[11] Bianco P. Bone and the hematopoietic niche: a tale of two stem cells. Blood 2011; 117: 5281-5288.
[12] Bihari C, Lal D, Thakur M, Sukriti S, Mathur D, Patil AG, Anand L, Kumar G, Sharma S, Thapar S, Rajbongshi A, Rastogi A, Kumar A and Sarin SK. Suboptimal level of bone-forming cells in advanced cirrhosis are associated with hepatic osteodystrophy. Hepatol Commun 2018; 2: 1095-1110.
[13] Caplan AI and Correa D. The MSC: an injury drugstore. Cell Stem Cell 2011; 9: 11-15.
[14] Murphy MB, Moncivais K and Caplan AI. Mesenchymal stem cells: environmentally responsive therapeutics for regenerative medicine. Exp Mol Med 2013; 45: e54.
[15] Parekkadan B, van Poll D, Megeed Z, Kobayashi N, Tilles AW, Berthiaume F and Yarmush ML. Immunomodulation of activated hepatic stellate cells by mesenchymal stem cells. Biochem Biophys Res Commun 2007; 363: 247-252.
[16] Fang B, Shi M, Liao L, Yang S, Liu Y and Zhao RC. Systemic infusion of FLK1(+) mesenchymal stem cells ameliorate carbon tetrachloride-induced liver fibrosis in mice. Transplantation 2004; 78: 83-88.
[17] Oyagi S, Hirose M, Kojima M, Okuyama M, Kawase M, Nakamura T, Ohgushi H and Yagi K. Therapeutic effect of transplanting HGF-treated bone marrow mesenchymal cells into CCl4-injured rats. J Hepatol 2006; 44: 742-748.
[18] Li T, Zhu J, Ma K, Liu N, Feng K, Li X, Wang S and Bie P. Autologous bone marrow-derived mesenchymal stem cell transplantation promotes liver regeneration after portal vein embolization in cirrhotic rats. J Surg Res 2013; 184: 1161-1173.
[19] Meier RP, Muller YD, Morel P, Gonelle-Gispert C and Buhler LH. Transplantation of mesenchymal stem cells for the treatment of liver diseases, is there enough evidence? Stem Cell Res 2013; 11: 1348-1364.
[20] Kim G, Eom YW, Baik SK, Shin Y, Lim YL, Kim MY, Kwon SO and Chang SJ. Therapeutic effects of mesenchymal stem cells for patients with chronic liver diseases: systematic review and meta-analysis. J Korean Med Sci 2015; 30: 1405-1415.
[21] Alfaifi M, Eom YW, Newsome PN and Baik SK. Mesenchymal stromal cell therapy for liver diseases. J Hepatol 2018; 68: 1272-1285.
[22] Suk KT, Yoon JH, Kim MY, Kim CW, Kim JK, Park H, Hwang SG, Kim DJ, Lee BS, Lee SH, Kim HS, Jang JY, Lee CH, Kim BS, Jang YO, Cho MY, Jung ES, Kim YM, Bae SH and Baik SK. Transplantation with autologous bone marrow-derived mesenchymal stem cells for alcoholic cirrhosis: phase 2 trial. Hepatology 2016; 64: 2185-2197.
[23] Mohamadnejad M, Alimoghaddam K, Bagheri M, Ashrafi M, Abdollahzadeh L, Akhlaghpoor S, Bashtar M, Ghavamzadeh A and Malekzadeh R. Randomized placebo-controlled trial of mesenchymal stem cell transplantation in decompensated cirrhosis. Liver Int 2013; 33: 1490-1496.
[24] Geiger H, de Haan G and Florian MC. The ageing haematopoietic stem cell compartment. Nat Rev Immunol 2013; 13: 376-389.
[25] Dominici M, Le Blanc K, Mueller I, Slaper-Cortenbach I, Marini F, Krause D, Deans R, Keating A, Prockop D and Horwitz E. Minimal criteria for defining multipotent mesenchymal stromal cells. The International Society for Cellular Therapy position statement. Cytotherapy 2006; 8: 315-317.
[26] Chen CT, Shih YR, Kuo TK, Lee OK and Wei YH. Coordinated changes of mitochondrial biogenesis and antioxidant enzymes during osteogenic differentiation of human mesenchymal stem cells. Stem Cells 2008; 26: 960-8.
[27] Pattappa G, Thorpe SD, Jegard NC, Heywood HK, de Bruijn JD and Lee DA. Continuous and uninterrupted oxygen tension influences the colony formation and oxidative metabolism of human mesenchymal stem cells. Tissue Eng Part C Methods 2013; 19: 68-79.
[28] Chen L, Chen R, Wang H and Liang F. Mechanisms linking inflammation to insulin resistance. Int J Endocrinol 2015; 2015: 508409.
[29] Divakaruni AS and Brand MD. The regulation and physiology of mitochondrial proton leak. Physiology (Bethesda) 2011; 26: 192-205.
[30] Tal MC, Sasai M, Lee HK, Yordy B, Shadel GS and Iwasaki A. Absence of autophagy results in reactive oxygen species-dependent amplification of RLR signaling. Proc Natl Acad Sci U S A 2009; 106: 2770-5.
[31] Shares BH, Busch M, White N, Shum L and Eliseev RA. Active mitochondria support osteogenic differentiation by stimulating β-catenin acetylation. J Biol Chem 2018; 293: 16019-16027.
[32] Killer MC, Nold P, Henkenius K, Fritz L, Riedlinger T, Barckhausen C, Frech M, Hackstein H, Neubauer A and Brendel C. Immunosuppressive capacity of mesenchymal stem cells correlates with metabolic activity and can be enhanced by valproic acid. Stem Cell Res Ther 2017; 8: 100.
[33] Kizilay Mancini O, Lora M, Cuillerier A, Shum-Tim D, Hamdy R, Burelle Y, Servant MJ, Stochaj U and Colmegna I. Mitochondrial oxidative stress reduces the immunopotency of mesenchymal stromal cells in adults with coronary artery disease. Circ Res 2018; 122: 255-266.

[34] Correia-Melo C and Passos JF. Mitochondria: are they causal players in cellular senescence? Biochim Biophys Acta 2015; 1847: 1373-9.
[35] Wiley CD, Velarde MC, Lecot P, Liu S, Sarnoski EA, Freund A, Shirakawa K, Lim HW, Davis SS, Ramanathan A, Gerencser AA, Verdin E and Campisi J. Mitochondrial dysfunction induces senescence with a distinct secretory phenotype. Cell Metab 2016; 23: 303-14.
[36] Nakchbandi IA. Osteoporosis and fractures in liver disease: relevance, pathogenesis and therapeutic implications. World J Gastroenterol 2014; 20: 9427-38.
[37] Assimakopoulos SF, Tsamandas AC, Tsiaoussis GI, Karatza E, Zisimopoulos D, Maroulis I, Kontogeorgou E, Georgiou CD, Scopa CD and Thomopoulos KC. Intestinal mucosal proliferation, apoptosis and oxidative stress in patients with liver cirrhosis. Ann Hepatol 2013; 12: 301-7.
[38] Shum LC, White NS, Mills BN, Bentley KL and Eliseev RA. Energy metabolism in mesenchymal stem cells during osteogenic differentiation. Stem Cells Dev 2016; 25: 114-22.
[39] An JH, Yang JY, Ahn BY, Cho SW, Jung JY, Cho HY, Cho YM, Kim SW, Park KS, Kim SY, Lee HK and Shin CS. Enhanced mitochondrial biogenesis contributes to Wnt induced osteoblastic differentiation of C3H10T1/2 cells. Bone 2010; 47: 140-50.
[40] Forni MF, Peloggia J, Trudeau K, Shirihai O and Kowaltowski AJ. Murine mesenchymal stem cell commitment to differentiation is regulated by mitochondrial dynamics. Stem Cells 2016; 34: 743-55.
[41] Fu X, Li Y, Huang T, Yu Z, Ma K, Yang M, Liu Q, Pan H, Wang H, Wang J and Guan M. Runx2/osterix and zinc uptake synergize to orchestrate osteogenic differentiation and citrate containing bone apatite formation. Adv Sci (Weinh) 2018; 5: 1700755.
[42] Chocarro-Calvo A, García-Martínez JM, Ardila-González S, De la Vieja A and García-Jiménez C. Glucose-induced β-catenin acetylation enhances Wnt signaling in cancer. Mol Cell 2013; 49: 474-86.
[43] Mailloux RJ and Harper ME. Mitochondrial proticity and ROS signaling: lessons from the uncoupling proteins. Trends Endocrinol Metab 2012; 23: 451-8.
[44] Kim J, Piao Y, Pak YK, Chung D, Han YM, Hong JS, Jun EJ, Shim JY, Choi J and Kim CJ. Umbilical cord mesenchymal stromal cells affected by gestational diabetes mellitus display premature aging and mitochondrial dysfunction. Stem Cells Dev 2015; 24: 575-586.

Table S1. Clinical and demographic feature of cirrhotic patients

Patient	Age	Gender	Etiology	CTP Score	MELD Score
D1	32	M	ALD	7	12
D2	42	M	CRY	8	15
D3	44	M	ALD	9	20
D4	33	M	ALD	9	19
D5	43	M	ALD	9	14
D6	49	M	ALD	10	16
D7	42	M	CRY	11	20
D8	48	M	ALD	8	13
D9	41	M	CRY	8	13
D10	39	M	ALD	8	18
Ave. (± SD)	41.3 (±5.4)	M	-	8.7 (±1.13)	16.2 (±2.3)
Normal Ave. (± SD)	40.25 (±4.2)	-	Healthy individuals	-	-

ALD - Alcoholic Liver disease; CRY - Cryptogenic; CTP - Child-Turcotte-Pugh; MELD - Model for End-Stage Liver Diseases.

A

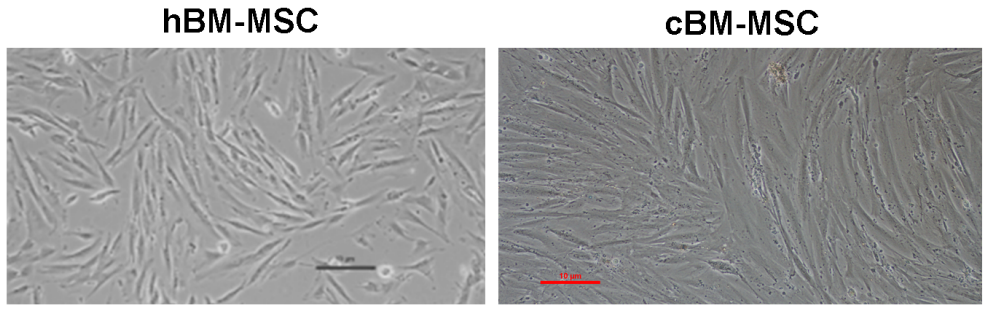

B

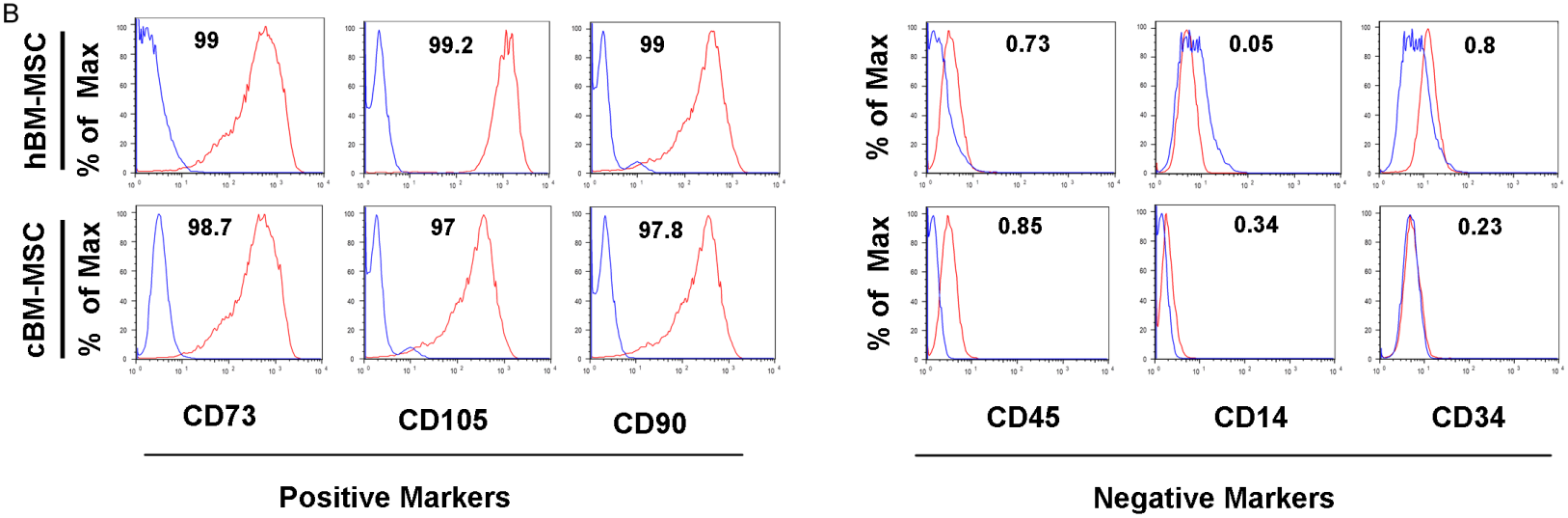

Markers	Positive Markers Average% ± SD			Negative Positive Markers average %± SD		
	CD73	CD105	CD90	CD45	CD14	CD34
hBM-MSC	96.9±2.9	97.8±1.7	95.5±2.5	0.93±0.4	0.6±0.3	1.7±1.3
cBM-MSC	96.5±3.6	97.6±1.9	95.2±3	0.98±0.3	0.56±0.34	1.62±1.7

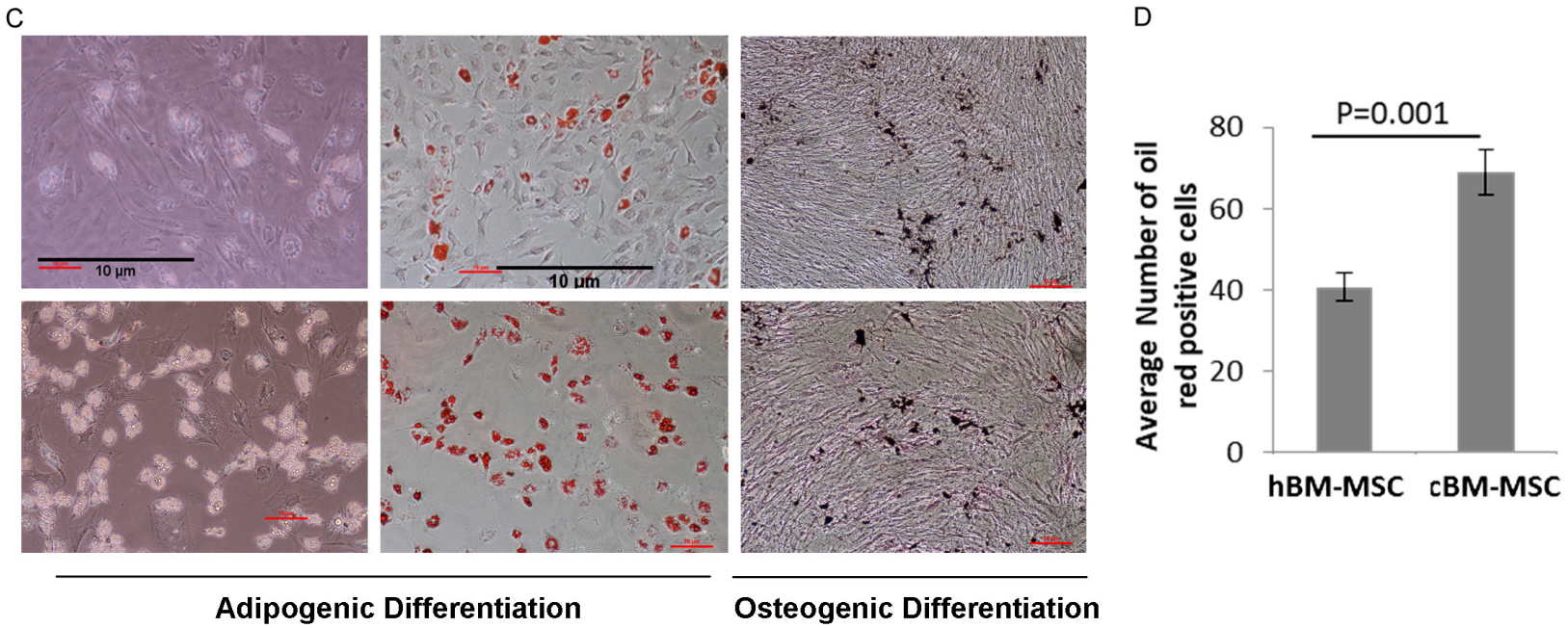

Figure S1. In-vitro characterization of minimal criteria for mesenchymal stem cells. A. Phage contrast photo showing morphology of hBM-MSCs and cBM-MSC (magnification 10×). B. Representative histogram (top) and table (bottom) showing Percentage positivity of surface marker expression in healthy (hBM-MSCs) and cirrhotic (cBM-MSCs) bone marrow MSCs (average % ± SD). C. Representative images of hBM-MSC and cBM-MSC differentiated into Adipocytes and osteocytes as visualized by Oil Red O and von Kossa stains respectively. D. Bar-Graph showing number of oil-red positive cells in hBM-MSCs and cBM-MSCs.

Table S3. Pathway analysis for the Genes differentially up - regulated in cBM-MSCs as compared hBM-MSCs

Up regulated genes					
Go-Biological					
	TERM	% Count	*P*-value	Combined Score	Genes
1	proteasome-mediated ubiquitin-dependent protein catabolic process (GO:0043161)	36.43%	7.12E-09	31.34745	UBXN2A; CCNF; UBE3A; PSMD8; PSMD9; PSMD6; PSMD7; KAT5; PSMD2; PSMD3; FBXO4; GTSE1; SKP1; FBXW5; FBXW7; FBXW11; UBE2E1; UBE4B; ARMC8; KCTD5; RNF126; CDC34; KCTD10; TBL1XR1; PSME3; HECW1; KCTD13; ANAPC4; ANAPC5; RBCK1; RNF122; RNF121; VCP; ANAPC15; PSMD13; CUL3; SEL1L; AGAP3; UBE2J2; UBE2J1; ANAPC11; CCNB1; SHARPIN; RNF216; BTBD1; TMEM129; BTBD2; PSMF1; UBE2C; WFS1; SMURF1; PLK1; BTBD6; UBE2A; KLHL20; FBXO31; NSFL1C; NPLOC4; DNAJC10; FBXL2; RNF187; RNF11; TNFAIP1; SEC61B; AXIN1; PPP2R5C; SIRT2; PSMA3; UBE2R2; NEMF; MAN1B1; DERL3; DERL1; RNF6; RNF4; PSMB6; FBXL20; RMND5B; ERLEC1; PSMB4; FZR1; PSMB5; C18ORF25; MTA1; RMND5A; RNF139; PSMB2; TBX21; SPOP; UBQLN1; DNAJB9; BUB3; DCAF11; FBXL19; SGTA; TMUB1; WWP1; FBXL18; UBE2G2; SPSB3; CUL4A; KBTBD4; PSMC5; PSMC6; JKAMP; CTNNB1
2	proteasomal protein catabolic process (GO:0010498)	36.29%	2.19E-07	25.52573	RNF11; UBXN2A; KEAP1; UBE3A; TNFAIP1; PSMD8; PSMD9; PSMD6; PSMD7; KAT5; PSMD2; PSMD3; GTSE1; SKP1; FBXW5; FBXW11; UBE2E1; DNAJB12; AXIN1; UBE4B; ARMC8; PPP2R5C; KCTD5; SIRT2; RNF126; PSMA3; CDC34; UBE2R2; KCTD10; TBL1XR1; PSME3; HECW1; KCTD13; ANAPC4; ANAPC5; RBCK1; RNF122; VCP; ANAPC15; PSMD13; CUL3; SEL1L; DERL1; RNF6; AGAP3; RNF4; FBXO44; ANAPC11; PSMB6; RMND5B; ERLEC1; PSMB4; PSMB5; C18ORF25; SHARPIN; MTA1; RMND5A; RNF216; RNF139; PSMB2; BTBD1; TBX21; BTBD2; SPOP; PSMF1; BUB3; DCAF11; ATE1; KLHL25; UBE2C; SMURF1; RHBDD1; FBXL19; WWP1; NR1D1; BTBD6; UBE2A; KLHL20; SPSB3; CUL4A; KBTBD4; NSFL1C; PSMC5; PSMC6; CTNNB1; RNF187
3	protein ubiquitination (GO:0016567)	31.23%	3.86E-07	21.15201	UBE3C; KLHL36; FBXO27; CCNF; RNF19B; KEAP1; CBLC; KLHDC7A; UBE3A; UBE3B; UBE2Z; KLHL30; UBE2L3; PSMD8; HERC5; PSMD9; PSMD6; PSMD7; RUSC1; PSMD2; PSMD3; FBXO4; FBXO7; TRIM21; SKP1; RNF43; MYLIP; FBXW5; USP5; FBXO18; FBXW7; FBXW11; UBE2E3; FBXW9; UBE2E1; MUL1; NOSIP; UBE4B; RC3H2; RNF126; RRAGA; CDC34; TRIM17; KCTD10; PSME3; HECW1; KCTD13; UBE2V2; RBCK1; RNF122; VCP; PSMD13; CUL3; UBR4; KLHL12; BCL10; UBE2J2; FBXO44; FBXO41; ANAPC11; BTBD1; BTBD2; TMEM129; PSMF1; LONRF1; BRAP; PHC1; KLHL25; BTBD18; KLHL26; UBE2C; SMURF1; SIAH2; PLK1; KLHL21; KLHL22; LNPEP; ISG15; BTBD6; UBE2A; KLHL24; FBXO31; KLHL20; UBOX5; MKRN1; UBE2O; BLMH; FBXL2; SAE1; FBXL4; RNF187; LRSAM1; RNF11; RNF13; TNFAIP1; KBTBD12; ARIH2; TRIM69; SHPRH; COMMD1; UCHL3; RNF168; TRAF7; PSMA3; UBE2R2; GAN; WAC; BIRC7; ZNF598; THOP1; RNF166; RNF31; HIST1H2BO; UHRF2; PELI3; PELI2; DERL1; RNF6; RNF4; RNF135; PSMB6; FBXL20; DCAF15; CAND2; RMND5B; PSMB4; PSMB5; C18ORF25; RMND5A; CAND1; RNF139; PSMB2; LEO1; SPOP; RBBP6; VHL; UBL4A; UBL4B; USP9X; RNF26; FBXL19; WWP1; FBXL18; FBXL16; UBE2G2; FBXL14; FBXL12; SPSB3; CUL4A; KBTBD4; PSMC5; PINK1; PSMC6; KLHL5; KLHL7; ASB9; TRIP12; KBTBD7
4	regulation of autophagy (GO:0010506)	35.96%	2.55E-06	21.24258	USP36; WDR41; PRKAG1; PRKAG2; PTPN22; PIK3CB; SOGA1; TRIM8; RUVBL1; MLST8; TLK2; AKT1; PIP4K2B; VPS35; PIP4K2C; ATP6V1E1; DNM1L; TRIM21; TRIM65; RAB8A; BOK; SREBF1; TMEM150B; ATP6V0B; TMEM150A; EXOC8; FBXW7; DAPK3; PRKAB1; ATG13; SIRT2; SREBF2; DCN; RRAGA; RRAGB; RRAGD; EXOC4; ULK2; ULK1; VDAC1; ATP6V0D1; DEPDC5; EXOC1; ATP6V1A; USP10; VPS26B; MEFV; C9ORF72; RASIP1; ABL1; TBC1D14; ATP6V0E2; ATP6V1D; ATP6V1C1; ATP6V0A1; SNX6; KDM4A; OSBPL7; BAD; BNIP3; SVIP; MTOR; TPCN1; TMEM59; DAP; PINK1; RHEB; TAB2; ATP13A2; FBXL2; LAMTOR1; LAMTOR4; LAMTOR5
5	vesicle-mediated transport (GO:0016192)	30.49%	2.16E-05	15.02448	VPS29; WIPF2; MLC1; FNBP1L; GOLGA4; ZFYVE27; TBC1D10C; VPS35; AGFG2; PLEKHJ1; MFSD2A; TBC1D10B; VPS18; RALBP1; VPS33B; SYTL1; TSC2; SCRIB; CSNK1D; VRK3; SYTL4; SYTL3; MAPK8IP1; ACAP3; RNF126; ACAP1; CTAGE5; KIF16B; RAB35; RIN3; TBC1D23; TSNARE1; CSNK1G2; STX1A; LRPAP1; MAGEL2; AGAP2; RHOBTB3; FAM109B; FAM109A; VPS26B; AGAP3; C2CD4C; ADRB2; C9ORF72; ADAP2; VPS11; SNX9; TBC1D17; EVI5; RAB6B; RAB11FIP3; SNX8; VTI1B; S100A10; GPIHBP1; SNX6; SPTBN2; UVRAG; RAB27B; SNF8; TVP23B; HSPA2; SYT8; SYT6; EHD1; FAM160A2; EHD3; SPIRE2; UBE2O; MON1A; DENND1C; DENND1A; SNX10; LRMP; SNX11; ACTR1A; AP1G2; TMED2; KIF1C; KIF1A; RAC1; BCAS3; AKTIP; RHOH; COMMD1; ARFGAP3; ARFGAP1; RHOB; ARL4C; RHOV; VAMP5; CHMP7; VAMP2; RHOQ; VAMP3; SEC22C; NAPA; SNAP47; BECN1; NAPB; VPS4A; TGFBRAP1; GOSR1; SNX33; ASAP2; CDC42; ARFRP1; CYTH2; VPS51; CUX1; VPS53; STX6; STX5; STX4; RILP; ATP9A; SPAG9; RAB11A; RAB11B; MYO1E; SGSM3; VPS41; RAB13; SMAP1
6	endosomal transport (GO:0016197)	32.75%	7.75E-05	14.21951	DENND1C; VPS29; DENND1A; TBC1D10C; VPS35; ANXA8; VPS36; AP5S1; TBC1D10B; PLEKHJ1; VPS18; AKTIP; VPS37C; SCRIB; VPS37B; RHOB; ARL4C; RNF126; ZFYVE16; WDR81; KIF16B; HGS; RAB35; TBC1D23; CHMP6; VPS25; CHMP7; VAMP3; BECN1; SDCCAG3; MAGEL2; TSG101; AP5Z1; VPS4B; VPS4A; TGFBRAP1; GOSR1; RHOBTB3; FAM109B; FAM109A; VPS26B; SNX33; ADRB2; C9ORF72; ARFRP1; AP5M1; VPS51; VPS53; MVB12B; VPS11; STX6; STX5; SNX9; TBC1D17; RAB11FIP3; RAB6B; EVI5; RILP; VTI1B; SNX6; SPAG9; SNF8; NSG1; RAB11B; KLHL20; EHD1; EHD3; FAM160A2; SNX17; VPS41; RAB13; CHMP2A; UBAP1; UBE2O; LAMTOR1

7	regulation of macroautophagy (GO:0016241)	37.07%	1.25E-04	15.28391	ATP6V1A; GPSM1; RAB1B; PRKAG1; PRKAG2; VPS26B; C9ORF72; MLST8; AKT1; TBC1D14; VPS35; QSOX1; ATP6V1E1; ATP6V0E2; ATP6V1D; ATP6V1C1; ATP6V0A1; SNX6; BNIP3L; ATP6V0B; EXOC8; BNIP3; TSC2; PRKAB1; ATG13; RAB33A; DCN; MTOR; RRAGA; PINK1; RRAGB; RHEB; RRAGD; EXOC4; WAC; TBC1D25; ULK1; ATP13A2; LAMTOR1; ATP6V0D1; LAMTOR4; EXOC1; LAMTOR5
8	positive regulation of exosomal secretion (GO:1903543)	66.67%	2.41E-04	25.47515	SDCBP; TSG101; PDCD6IP; SDC4; HGS; VPS4B; VPS4A; CHMP2A; ATP13A2; SNF8
9	regulation of ubiquitin-protein transferase activity (GO:0051438)	51.61%	2.53E-04	19.60422	ZYG11B; ZER1; FEM1A; FBXW7; LIMK1; PLK1; DCUN1D1; AXIN1; DCUN1D2; PARK7; UBE2L3; PINK1; BAG5; ABL1; PIN1; TRIB3
10	regulation of vesicle-mediated transport (GO:0060627)	34.78%	3.07E-04	12.90676	NRP1; HIP1; GOSR1; SNX12; TBC1D3C; CPLX1; RAB40A; RAB40B; RNF139; TBC1D10C; ABL1; AP2S1; TBC1D14; STX4; TBC1D17; TBC1D22A; EVI5; TBC1D15; RAB8A; CD177; TBC1D10B; TBC1D16; PACSIN1; MAPK3; UVRAG; PTPN1; MAP2K1; RABGAP1L; RAB4A; MAP2K2; GRTP1; HIP1R; TSC2; ARFGAP1; RAB11A; RAB11B; TBC1D1; TBC1D2; PINK1; ZFYVE16; SNX17; SGSM3; SGSM2; RAB13; TBC1D25; LLGL1; VAMP2; LLGL2

Go-Molecular

	TERM	% Count	*P*-value	Combined Score	Genes
1	ubiquitin-protein transferase activity (GO:0004842)	30.70%	1.21E-05	15.94382	UBE3C; KLHL36; FBXO27; CCNF; RNF19B; KEAP1; CBLC; CBLB; KLHDC7A; UBE3A; UBE3B; UBE2Z; KLHL30; UBE2L3; HERC5; TRIM28; FBXO4; FBXO3; FBXO7; TRIM21; SKP1; RNF43; MYLIP; FBXW5; FBXW7; FBXW11; UBE2E3; FBXW9; UBE2E1; MUL1; NOSIP; RC3H2; RNF126; CDC34; TRIM17; KCTD10; HECW1; KCTD13; UBE2V2; ANAPC4; ANAPC5; RBCK1; RNF122; RNF121; MAGEL2; CUL3; UBR4; KLHL12; UBE2J2; DTX4; FBXO44; FBXO41; ANAPC11; UBE2J1; SHARPIN; RNF216; TMEM129; LONRF1; BRAP; UBE2F; BTBD18; KLHL26; UBE2C; SMURF1; SIAH2; KLHL21; KLHL22; UBE2A; KLHL24; FBXO31; KLHL20; MKRN1; UBE2O; FBXL2; FBXL4; RNF187; LRSAM1; RNF11; RNF13; TNFAIP1; KBTBD12; TRIM5; ARIH2; TRIM69; ZYG11B; SHPRH; ZER1; AKTIP; RNF168; TRAF7; UBE2R2; TRAF3; GAN; BIRC7; ZNF598; RNF166; RNF31; UHRF2; PELI3; PELI2; RNF6; DCST1; RNF4; RNF135; FBXL20; CDC42; RMND5B; C18ORF25; RMND5A; RNF139; RBBP6; VHL; FEM1A; RNF26; FBXL19; WWP1; FBXL18; FBXL16; UBE2G2; FBXL14; FBXL12; SPSB3; CUL4A; KLHL5; KLHL7; TRIP12; KBTBD7; ASB3
2	ubiquitin protein ligase binding (GO:0031625)	30.99%	1.82E-04	12.2396	PTPN22; CASC3; UBE2Z; UBE2L3; MAP1LC3B; TRIM28; SUMO1; MAP1LC3C; CASP10; SLC22A18; SUMO2; UBXN7; DNM1L; FBXO7; KCNH2; GABARAPL2; CCT2; SHPRH; FBXW7; AKTIP; USP2; AXIN1; MUL1; TRAF1; SCAMP3; RRAGA; CDC34; UBE2R2; TRAF3; UBE2V2; TRIB3; TRIB2; VCL; RNF31; BECN1; VCP; TSG101; RALB; CUL3; DERL1; DTX1; PRR5L; BCL10; NLK; UBE2J2; GABARAP; RELA; EGFR; UBE2J1; NKD2; BAG5; BTBD1; PRKAR2A; BTBD2; SPOP; SNX9; RIPK1; UBL4A; UBE2F; SMAD2; HSPA9; UBL4B; KDM4A; USP25; EGR2; JUN; XRCC5; UBE2C; WFS1; NEK6; HSPA6; RPA2; ISG15; UBE2G2; BTBD6; UBE2A; PRDX6; CUL4A; KBTBD4; PER1; UBOX5; PINK1; NPLOC4; MC1R; ABI2; JKAMP; UBE2O; ASB3
3	phosphatidylinositol phosphate binding (GO:1901981)	39.51%	2.33E-04	15.16193	DENND1C; PLEKHF2; HIP1; PLEKHB2; DENND1A; SNX13; SNX11; IQGAP2; JPH2; ADAP2; SAP30L; SH3PXD2B; AKT1; ARFIP1; ANXA8; BBS5; PHLDA3; GSDMD; GSDMB; HIP1R; WIPI1; PLEKHA3; WIPI2; COMMD1; PLEKHA4; SNX20; GOLPH3; ZFYVE16; KIF16B; PARD3; BTK; TECPR1
4	ubiquitin-like protein ligase binding (GO:0044389)	30.30%	3.59E-04	11.02783	PTPN22; CASC3; UBE2Z; UBE2L3; MAP1LC3B; TRIM28; SUMO1; MAP1LC3C; CASP10; SLC22A18; SUMO2; UBXN7; DNM1L; FBXO7; KCNH2; GABARAPL2; CCT2; SHPRH; FBXW7; AKTIP; USP2; AXIN1; MUL1; TRAF1; SCAMP3; RRAGA; CDC34; UBE2R2; HGS; TRAF3; UBE2V2; TRIB3; TRIB2; VCL; RNF31; BECN1; VCP; TSG101; RALB; CUL3; DERL1; DTX1; PRR5L; BCL10; NLK; UBE2J2; GABARAP; RELA; EGFR; UBE2J1; NKD2; CCNB1; BAG5; BTBD1; PRKAR2A; BTBD2; SPOP; SNX9; RIPK1; UBL4A; UBE2F; SMAD2; HSPA9; UBL4B; KDM4A; USP25; EGR2; JUN; XRCC5; UBE2C; WFS1; NEK6; HSPA6; RPA2; ISG15; UBE2G2; BTBD6; UBE2A; PRDX6; CUL4A; KBTBD4; PER1; UBOX5; PINK1; NPLOC4; MC1R; ABI2; JKAMP; UBE2O; ASB3
5	phosphatase binding (GO:0019902)	36.27%	5.81E-04	12.39791	VCP; ELL; EGFR; SLC9A3R1; PPP3R1; CNST; CHCHD3; PPME1; ANKAR; MAP2K7; MAP3K5; MAPK3; SMAD2; PPP1R26; PPP1R27; FCRL3; SIGLEC10; STAT3; TSC2; RPA2; VRK3; GTF2F1; MAPK14; DLG1; CEACAM1; WNK1; DLG4; TRAF3; RCAN3; CRY2; CRY1; ANAPC4; CTNNB1; ANAPC5; FBXL2; PPP1R12B; PPP1R12C
6	phosphatidylinositol-3-phosphate binding (GO:0032266)	48.39%	9.49E-04	15.44851	PLEKHF2; HIP1; DENND1A; SNX13; WIPI1; WIPI2; PLEKHA4; SNX20; JPH2; KIF16B; PARD3; SH3PXD2B; BBS5; TECPR1; PHLDA3
7	hydrolase activity, acting on carbon-nitrogen (but not peptide) bonds, in linear amides (GO:0016811)	37.33%	0.001565	11.06275	KDM1A; HDAC1; HDAC11; NGLY1; HDAC9; PHF21A; GLS; NDST2; MTA1; PDF; RBBP4; NACC2; AMDHD2; MIER2; SAP30L; SAP18; RBBP7; DARS; NTAN1; SIRT2; SAP30; ACR; ACER2; FA2H; BTD; BRMS1; VNN2; RCOR1

8	ubiquitin binding (GO:0043130)	38.71%	0.001868	11.15589	RNF31; USP25; TSG101; USP5; UBXN2A; UBE2A; UCHL3; SIRT2; UBAC2; RNF168; NSFL1C; SHARPIN; NPLOC4; WDR92; RNF216; DDI2; TOLLIP; UBXN7; UBAP1; RBCK1; BUB3; VPS36; FBXO7; RAE1
9	purine ribonucleoside triphosphate binding (GO:0035639)	28.03%	0.001892	8.061911	CARS; SMC4; YARS2; GIMAP7; THG1L; TUBB6; PPIP5K1; AKT2; AKT3; TUBB1; PIM1; LONP1; AKT1; MAP3K6; PDK2; MAP3K5; ACVR1; ABCG5; DAPK3; RUNX3; GTPBP4; MSH6; RRAGA; RAB31; RRAGB; RAB35; RRAGD; BTK; SIK1; TSSK2; ARL8B; BRSK1; GNAZ; RHOBTB3; WNK4; ARL2; ABCB9; NLK; RHOBTB1; RHOBTB2; RHOT1; NUAK2; PMVK; ABL1; HSPA9; RAB4A; EIF2B2; DMPK; HSPA4; NEK6; PLK1; HSPA6; RAB27B; HSPA2; GNAO1; PPP5C; CDK6; RHEB; WNK1; NVL; DIRAS2; MAST1; PRKAG1; OLA1; PRKAG2; RND2; TUBA1C; TUBA1A; TLK2; TLK1; RAC1; RAB8A; MAP4K1; MAP4K2; SPHK1; RHOH; OXSR1; RHOC; SYN1; NME1; RHOB; RAP2A; RAP2B; OAS1; MCM6; RHOV; RHOQ; PDXK; RALB; RAB1B; VPS4A; IGHMBP2; ATP1A3; RECQL4; CDC42; TUBA3E; MTHFD1L; MKNK2; MAP4K5; MAP4K4; KCNJ11; GSS; CDC42BPB; TUBB4B; CDC42BPA; RAB11B; BCKDK; PINK1; RIT1; P2RX4; RAB13
10	ubiquitin protein ligase activity (GO:0061630)	30.73%	0.002387	8.510853	LRSAM1; RNF11; UBE3C; CBLC; RNF19B; CBLB; UBE3A; UBE3B; UBE2Z; HERC5; ARIH2; SKP1; RNF43; MYLIP; SHPRH; AKTIP; NOSIP; UBE4B; RNF126; CDC34; UBE2R2; HECW1; UBE2V2; ANAPC5; ZNF598; RNF122; RNF166; RNF121; UHRF2; CUL3; PELI3; PELI2; RNF6; UBE2J2; RNF4; DCST1; UBE2J1; ANAPC11; CDC42; C18ORF25; RNF216; RNF139; TMEM129; RBBP6; VHL; LONRF1; BRAP; UBE2F; UBE2C; SMURF1; RNF26; WWP1; UBE2A; UBE2G2; CUL4A; UBOX5; MKRN1; UBE2O; TRIP12

Go Cellular

	TERM	% Count	*P*-value	Combined Score	Genes
1	recycling endosome (GO:0055037)	38.66%	2.19E-05	19.02069	SDCCAG3; MCTP1; TFRC; MLC1; FAM109B; FAM109A; NDRG1; ZFYVE27; TUBA1A; GGA3; VPS51; VPS53; TBC1D14; RAC1; TBC1D17; LDLRAP1; RAB11FIP3; RAB8A; ATP9A; PLEKHJ1; VTI1B; BOK; FZD7; SLC11A2; HLA-B; NSG1; SNF8; COMMD1; HLA-G; TMEM230; RAB11A; SCAMP2; RAB11B; EHD1; FCHSD1; EHD3; TF; RAP2A; RAP2B; GPR161; RAB35; SLC9A9; RAB13; ULK1; TUBGCP4; VAMP3
2	chromatin (GO:0000785)	32.09%	2.33E-05	15.70284	TOP2B; ELL; KDM1A; CITED2; SUV39H1; AKAP8L; HIST2H2AB; JMJD1C; PSIP1; CHD5; HR; PARK7; SMC3; LOXL2; MECP2; CHAF1A; EME2; MYC; DPF2; HIST1H1D; PMEPA1; UTY; BAHCC1; HIST1H2AC; PELP1; KDM6B; UPF1; BCAS3; MEF2C; DFFA; TBP; FBXO18; H2AFY; H2AFZ; BUD31; TCF12; H2AFX; RUNX3; LEMD2; HIC1; RBL2; MAF; RBL1; WDR82; RARA; PADI2; CHMP7; ASF1A; MCM2; L3MBTL1; KMT2E; ANKRD17; MAGED1; WBP2; HDAC1; SRF; RELA; MUC1; RBBP4; NACC2; TNRC18; E2F4; MEF2D; SMAD2; MBD4; KLHDC3; CBX7; JUN; JUND; KDM4C; POLR3GL; CBX3; STAT3; XRCC1; NR1H3; RPA2; NFATC1; NR1D1; UBE2A; KLF4; SMARCA2; GATAD2B; KLF1; ASXL1; H1F0; FER; PINK1; MIS18A; HIST3H2A; H2AFY2; NASP; CHMP2A; POLR3G; EIF3E; EZH2
3	nuclear speck (GO:0016607)	31.76%	4.05E-05	14.73365	USP36; MOCS2; GTF2H2C; ELL; TMEM179B; AKAP8L; GPATCH2; FAM107A; CHD5; SMC4; PQBP1; EFTUD2; ADAMTS4; SAP130; HABP4; TRIM69; POLI; PPP1R16B; BNIP3L; MEF2C; RBM15; IL15; SLC34A1; TCF12; H2AFX; DYRK1A; PRPF4B; TFIP11; HAUS6; KIF22; CDYL; GCAT; CKAP4; REXO4; ITPKC; PRPF4; DDX39A; CDC34; THAP7; PRPF3; CRY2; SRSF2; AAGAB; PPIG; SGK1; CACTIN; RAF1; SLU7; SRSF8; FTO; SF3B2; AP5Z1; RBM8A; POLDIP3; PRCC; POMP; ARHGAP18; U2AF1; FOXO4; GTF2E2; TIMM50; DPP3; GRK5; TBXA2R; U2AF2; PPP1R8; EP400; ZC3H18; LPXN; SAP18; RBBP6; SF3B1; S100PBP; ATP6V0A1; HEXIM2; MBD4; WTAP; API5; ZBTB16; LIMK1; CWC15; MAPK14; NFATC4; SMU1; FIBP; SNW1; WT1; APEX1; ZNF217; HBP1; TRIP12; PRPF31; CDK12; FBXL4
4	cullin-RING ubiquitin ligase complex (GO:0031461)	34.25%	7.46E-05	14.9317	KLHL36; PDCD6; FBXO27; CCNF; KEAP1; KLHDC7A; TNFAIP1; DCAF5; KLHL30; DDA1; KBTBD12; FBXO4; ARIH2; FBXO7; TRIM21; SKP1; ZYG11B; FBXW5; ZER1; FBXO18; FBXW7; FBXW11; COMMD1; KCTD5; KCTD10; GAN; KCTD13; ANAPC4; ANAPC5; ANAPC13; ANAPC15; CUL3; KLHL12; FBXO44; ANAPC11; FBXL20; DCAF15; DCAF16; FZR1; CAND1; BTBD1; BTBD2; SPOP; DCAF11; KLHL25; KLHL26; UBE2C; BTBD18; FBXL19; KLHL21; KLHL22; BTBD6; KLHL24; KLHL20; FBXO31; CUL4A; SPSB3; KBTBD4; KLHL5; KLHL7; FBXL2; KBTBD7
5	early endosome (GO:0005769)	32.43%	1.50E-04	13.10387	NRP1; SNX12; MLC1; SNX13; RUSC1; PMEPA1; VPS35; LDLRAP1; WLS; PLEKHJ1; BOK; MAP2K1; MAP2K2; MMGT1; SLC11A2; F2R; VPS33B; HLA-B; APOA1; COMMD1; KREMEN2; HLA-G; ZFYVE16; RAB31; WDR81; ALS2; KIF16B; HGS; WDFY1; RIN3; WDFY2; ATP6V0D1; LLGL1; VAC14; SDCCAG3; TSG101; USP10; VPS4A; TGFBRAP1; FAM109B; FAM109A; VPS26B; TM9SF4; EGFR; PRDX3; GGA3; RAP1A; VPS8; MVB12B; VPS11; STX6; APOE; SNX8; FCGR1B; ATP9A; VTI1B; SNX6; TBC1D16; MAPK3; TMEM184A; UVRAG; PTPN1; RABGAP1L; RAB4A; WNT3A; LNPEP; NSG1; SNX20; TMEM230; EHD1; TF; SNX17
6	clathrin adaptor complex (GO:0030131)	64.71%	1.72E-04	25.73483	AFTPH; HIP1; AP1G2; SYNRG; HIP1R; AP2S1; AP1S1; LDLRAP1; AP2A2; EGFR; SLC18A3

7	mitochondrion (GO:0005739)	26.41%	1.83E-04	10.42652	IFI27L2; ATP5C1; ABAT; GHITM; MTFR1L; GLS; ELK3; LACTB; CYP2D6; ZMIZ2; LONP1; VPS35; MPV17; FBXO7; PDK2; HEMK1; CMC2; SLC11A2; ACSL5; PRKCA; HOGA1; ATG13; CPT1B; GCAT; PISD; GTPBP3; CYP27A1; LARS2; NIF3L1; HOXB9; WDR81; KARS; MTHFD2; SUCLG2; VDAC1; TMEM126B; LETMD1; AURKAIP1; MMADHC; PTGES; SLC22A4; GCDH; AGAP2; ATP5J; CEND1; ATP5I; MRPL15; MRPL10; C12ORF65; PRDX3; MRPL20; CYB5R1; FAM124B; RHOT1; NTHL1; PTPMT1; BLOC1S2; TNRC18; ARGLU1; DECR1; PCK2; PRELID1; PYCR1; ERAL1; MRPL23; KIAA0391; PRDX6; FIBP; ALDH6A1; ECHDC2; ALDH18A1; SLC35F6; COX7B; MRPS15; SLC44A1; YJEFN3; HCCS; MRPL37; MYOM2; BBC3; MAP1LC3B; AKAP10; AIFM3; MTG1; PCF11; MRPS26; PARP1; ACAD9; MRPS2; MRPL45; MRPL46; MRPS5; SREBF2; UCHL5; SIRT3; MRPL44; HADHB; SDHAF2; IVD; DLD; PLIN5; KANK2; ARMS2; DTYMK; GSTP1; TIMM13; IFI6; DLST; GRAMD4; NAPG; TMEM71; TRAK2; PDF; PDPR; MTHFD1L; MINOS1; NT5M; BRD8; C21ORF33; TIMMDC1; GSR; TRMT1; COX6C; TFAP4; APEX1; ZNF217; MSRB3; CRAT; SLC27A1; OXNAD1; NDUFA12; NDUFA10; PARK7; CELSR1; YARS2; TOMM20; TXN2; THG1L; PPP1CC; MTRF1; CHCHD3; MPC1; MPC2; NARS2; PMPCB; PMPCA; SLC25A42; HADH; TNFRSF4; TGM2; BNIP3L; MAP2K1; DGAT2; AGTPBP1; MAP2K2; ADPRHL2; PUS1; MUL1; SDHC; SDHD; SDHA; ATAD3A; SDHB; SLC9B2; PPIF; RAF1; DAP3; NDRG4; ENY2; NDUFB11; FOXO3; HIGD1A; TIMM50; BCL2L13; BAG5; NACC2; NLRP5; ABL1; COX14; RIPK1; TPPP; COA4; HSPA9; TFAP2C; PDHA1; SMURF1; CHCHD10; TIMM44; CWC15; ACSF3; NFKB1; COQ4; MAVS; TMEM11; CYP11B2; PXMP2; CYCS; DEGS1; MCU; BCL2L1; MIPEP; SLC25A3; MCUR1; ALAS1; COX4I1; RMND1; LRRK1; ACSM2A; ETFB; HK1; TCHP; MRPL3; HEBP2; CPT2; CASP4; ME3; MRPL9; DNM1L; HIBCH; BOK; TSFM; MARS2; AMT; NDUFC1; TNFRSF1A; SLC25A16; SMDT1; TST; NDUFS5; NDUFS4; DNLZ; TNFRSF25; PFDN2; CASQ1; SLC25A11; DDX28; BECN1; POLDIP2; RAP1GDS1; MTIF2; MTIF3; FTHL17; MRM1; SLC25A26; POLD4; ALDH1B1; STOM; D2HGDH; ROMO1; VHL; SLC25A23; SLC25A24; SNCA; MAPK3; METAP1D; PTCD1; PTCD2; NDUFA4; TXNRD2; BAD; BNIP3; TXNRD1; NDUFA1; KIAA1683; SUOX; GFER; GDAP1; SOD1; BCKDK; PINK1; GOLPH3
8	integral component of Golgi membrane (GO:0030173)	47.50%	2.78E-04	17.84048	SLC35B2; UBIAD1; ENTPD4; GALNT2; SLC35B1; CSGALNACT2; TEX261; SLC39A13; PCSK7; TVP23B; IER3IP1; YIF1B; ACER2; TBC1D20; RER1; CHST12; QSOX1; QSOX2; A4GALT
9	clathrin-coated vesicle (GO:0030136)	37.00%	3.73E-04	13.39587	HIP1; TFRC; DENND1A; CLTB; FAM109B; CLTA; FAM109A; CD3G; ADRB2; SLC2A4; CD3D; AP2A2; EGFR; FCHO2; STX6; AP2S1; SNX9; LDLRAP1; RAB8A; SLC18A3; EGF; VPS33B; SFTPD; HIP1R; RAB27B; EPN3; MYO1E; TF; MALL; RAB35; VPS41; RAB13; AVP; SFTPA1; IL7R; VAMP2; VAMP3
10	recycling endosome membrane (GO:0055038)	44.68%	3.88E-04	16.09874	FZD7; HLA-B; NSG1; NDRG1; HLA-G; RAB11A; SCAMP2; RAB11B; EHD1; RAP2A; EHD3; GGA3; ZFYVE27; RAP2B; RAB35; RAC1; RAB-11FIP3; RAB8A; VTI1B; BOK; VAMP3

KEGG PATHWAYS

	TERM	% Count	*P*-value	Combined Score	Genes
1	VEGF signaling pathway	44.07%	1.09E-04	18.44651	PXN; PIK3CB; PTGS2; CDC42; PPP3CB; PPP3R1; AKT2; AKT3; PLCG2; AKT1; RAC3; RAC1; PLCG1; MAPK3; MAP2K1; MAP2K2; SPHK2; BAD; NOS3; SPHK1; PLA2G4C; PRKCA; MAPK14; PTK2; MAPK13; RAF1
2	Endocytosis	31.56%	2.39E-04	12.07315	ARF3; VPS29; TFRC; WIPF2; CLTB; SNX12; CBLC; CLTA; CBLB; AP2A2; IGF1R; ZFYVE27; CAPZB; CHMP1B; VPS35; LDLRAP1; VPS36; RAB8A; PSD; PDCD6IP; HLA-B; VPS37C; EPS15L1; VPS37B; ARFGAP3; HLA-G; ARFGAP1; EPN1; EPN3; ACAP3; ZFYVE16; RAB31; ACAP1; HGS; PARD3; RAB35; CHMP6; VPS25; CHMP7; ARF5; TSG101; VPS4B; VPS4A; AGAP2; VPS26B; AGAP3; ASAP2; IL2RG; PRKCZ; EGFR; PLD2; CDC42; CYTH2; GRK5; CXCR2; MVB12B; AP2S1; RAB11FIP3; SNX6; SMAD2; RAB4A; SMURF1; IQSEC3; HSPA6; WWP1; SNF8; HSPA2; RAB11A; RAB11B; EHD1; EHD3; ARPC3; CAPZA2; CHMP2A; FGFR3; SMAP1; FOLR1
3	Platelet activation	35.48%	3.26E-04	13.06656	MYLK2; ITGA2B; ADCY4; ADCY3; PIK3CB; RASGRP2; PRKCZ; PIK3CG; ADCY6; MYLK; MYLK4; MYL12B; PTGS1; PPP1CC; RAP1A; TBXA2R; AKT2; PRKACG; AKT3; PLCG2; AKT1; MAPK3; P2RY12; FGA; NOS3; F2R; PLA2G4C; GP1BA; GP6; MAPK14; GP5; MAPK13; COL1A1; APBB1IP; GP9; PLCB3; COL3A1; COL1A2; GNAQ; TBXAS1; BTK; ORAI1; LCP2; F2RL3
4	mTOR signaling pathway	33.55%	5.38E-04	11.58458	PRR5; IRS1; FZD10; PIK3CB; IGF1R; AKT2; AKT3; MLST8; AKT1; ATP6V1E1; MAP2K1; SEC13; MAP2K2; MIOS; STRADA; PDPK1; TSC2; PRKCA; TNFRSF1A; SLC7A5; RRAGA; RRAGB; RRAGD; TBC1D7; ULK2; ULK1; RAF1; DEPDC5; SGK1; SOS2; ATP6V1A; DVL1; WNT1; AT-P6V1D; FNIP2; EIF4E; ATP6V1C1; WNT3; ATP6V1F; MAPK3; WNT10A; WNT3A; FZD7; WNT7B; FZD9; WNT7A; MTOR; RHEB; LAMTOR1; LAMTOR4; LAMTOR5
5	TNF signaling pathway	34.55%	0.001423	10.38698	CSF1; CXCL1; PIK3CB; PTGS2; CX3CL1; CXCL5; RELA; ICAM1; CREB3L3; CASP10; AKT2; CCL5; AKT3; AKT1; MAP3K8; RIPK1; FADD; MAP2K7; DNM1L; MAP3K5; MAP2K6; MAPK3; MAP2K3; MAP2K1; JUN; RIPK3; IL15; LIF; VEGFC; TRAF1; CFLAR; MAPK14; NFKB1; TNFRSF1A; MAPK13; MMP14; TRAF3; TAB2
6	Amino sugar and nucleotide sugar metabolism	41.67%	0.001544	12.37302	TSTA3; GALT; CMAS; UXS1; HEXB; MPI; PMM2; RENBP; HK1; CHIT1; CYB5R1; CYB5R4; GMDS; AMDHD2; UAP1L1; GMPPA; PGM2; NANS; FUK; PGM1
7	HIF-1 signaling pathway	35.00%	0.001664	10.27298	CAMK2B; TFRC; SLC2A1; PIK3CB; ENO2; RELA; EGFR; IGF1R; HK1; AKT2; AKT3; MKNK2; PLCG2; AKT1; PLCG1; VHL; EIF4E; MAPK3; EGLN1; MAP2K1; EGLN3; MAP2K2; PDHA1; NOS2; IFNGR1; EGF; NOS3; IFNGR2; STAT3; PRKCA; NFKB1; MTOR; TF; ALDOA; TLR4

8	Insulin resistance	34.26%	0.00193	9.822487	PYGB; SLC27A1; IRS1; SLC2A1; PRKAG1; PRKAG2; IRS2; SLC2A4; PIK3CB; PRKCZ; PTPRF; RELA; PPP1CC; GYS1; CREB3L3; AKT2; AKT3; AKT1; PPARGC1B; PCK2; SREBF1; PTPN1; PDPK1; NOS3; NR1H2; STAT3; NR1H3; PTPN11; PRKAB1; CPT1B; NFKB1; MTOR; TNFRSF1A; G6PC3; TRIB3; SLC27A3; SLC27A5
9	Insulin signaling pathway	32.12%	0.003247	8.441773	PYGB; IRS1; SHC1; PRKAG1; PRKAG2; CBLB; IRS2; SLC2A4; PIK3CB; PRKCZ; PTPRF; CRKL; HK1; PPP1CC; GYS1; AKT2; PRKACG; PRKAR2A; AKT3; MKNK2; PHKG2; AKT1; INPP5K; EIF4E; PCK2; MAPK3; SREBF1; PTPN1; MAP2K1; MAP2K2; PDPK1; BAD; TSC2; PRKAB1; MTOR; G6PC3; PRKAR1B; RHEB; CALM3; RAF1; SOS2; FBP1; CRK; RHOQ
10	Cellular senescence	30.63%	0.005672	7.266096	TRAF3IP2; PIK3CB; PPP1CC; PPP3CB; MYC; AKT2; AKT3; AKT1; MAP2K3; MAP2K1; MAP2K2; FBXW11; HLA-B; HUS1; TSC2; HLA-G; CDC25A; RBL2; RBL1; VDAC3; VDAC1; RAF1; CACNA1D; LIN9; FOXO3; KIR2DL3; ZFP36L2; RELA; PPP3R1; CCNB1; RRAS; RBBP4; E2F4; MAP2K6; MAPK3; SMAD2; GADD45B; CDKN2A; NFATC1; MAPK14; NFKB1; MTOR; NFATC4; MAPK13; CDK6; RHEB; CALM3; MCU; ATR

Table S4. Pathway analysis for the Genes differentially dow - regulated in cBM-MSCs as compared hBM-MSCs

Down regulated genes

Go Biological

	Term	% Count	*P*-value	Combined Score	Genes
1	negative regulation of cell morphogenesis involved in differentiation (GO:0010771)	20%	0.001604	29.62234	RTN4R; KANK1; RUFY3; TACSTD2; RAPGEF2; AP1AR
2	sister chromatid segregation (GO:0000819)	19%	0.002273	26.26527	TOP2A; CEP57; LATS1; ESPL1; TUBG1; RAN
3	chromosome organization (GO:0051276)	18%	0.000132	36.7203	TOP2A; LATS1; HHEX; CENPV; HIST1H4A; HIST1H3A; MSH3; XPA; HMGA2; XPC
4	DNA duplex unwinding (GO:0032508)	17%	0.001761	24.91899	RAD50; ERCC3; DDX1; DDX11; XPA; XPC; ASCC3
5	microtubule cytoskeleton organization involved in mitosis (GO:1902850)	16%	0.002682	21.6799	ESPL1; STMN1; BCCIP; RCC1; TUBG1; RAN; AURKA
6	tRNA aminoacylation for protein translation (GO:0006418)	15%	0.003476	19.82952	SARS2; LARS; PPA1; DARS2; TARS2; HARS; CARS2
7	mitotic spindle organization (GO:0007052)	14%	0.001316	20.63087	STMN1; BCCIP; RCC1; BIRC5; MYBL2; TUBG1; MAP9; RAN; BIRC3; AURKA
8	mitotic nuclear division (GO:0140014)	12%	0.004663	15.02568	CEP57; ESPL1; BCCIP; BIRC5; MYBL2; TUBG1; MAP9; RAN; BIRC3
9	cell cycle G1/S phase transition (GO:0044843)	12%	0.00212	16.94066	LATS1; POLE4; RANBP1; CDKN1B; MCM7; RPS6KB1; ORC2; CUL1; RCC1; BCAT1; ACVR1B
10	G1/S transition of mitotic cell cycle (GO:0000082)	11%	0.002006	16.33859	LATS1; POLE4; RANBP1; CDKN1B; RRM2; MCM7; RPS6KB1; ORC2; CUL1; RCC1; BCAT1; ACVR1B

Go Molecular

	Term	% Count	*P*-value	Combined Score	Genes
1	cAMP response element binding (GO:0035497)	57%	0.000112	119.696	CREB1; CREB3L2; HMGA2; E4F1
2	single-stranded DNA endodeoxyribonuclease activity (GO:0000014)	43%	0.002509	59.06336	RAD50; DCLRE1C; SETMAR
3	transcription factor activity, RNA polymerase II transcription factor recruiting (GO:0001135)	38%	0.003885	47.9064	DMTF1; CDC5L; MYBL2
4	cAMP binding (GO:0030552)	29%	0.001324	50.83955	POPDC3; PDE4B; RAPGEF2; HCN1
5	DNA replication origin binding (GO:0003688)	25%	0.013399	24.81352	DDX11; ORC2; HSPD1
6	methyl-CpG binding (GO:0008327)	20%	0.009828	21.2775	CHTOP; UHRF1; PRMT1; WDR77
7	tRNA binding (GO:0000049)	16%	0.005554	18.87182	MRPS27; ALKBH1; IFIT5; DARS2; HSD17B10; ALKBH8
8	aminoacyl-tRNA ligase activity (GO:0004812)	15%	0.008105	16.21797	SARS2; LARS; DARS2; TARS2; HARS; CARS2

9	transcriptional activator activity, RNA polymerase II transcription regulatory region sequence-specific binding (GO:0001228)	7%	0.012716	7.428279	MEF2A; ZBTB17; EBF2; HMGA2; CDC5L; USF1; CTCFL; CREB1; NFIB; TLX2; ELF4; IRF4; DDIT3; CREB3L2; REL; MYBL2; E2F3; MZF1; SOX4; ATF3; VENTX
10	RNA binding (GO:0003723)	6%	8.17E-05	14.05742	TOP2A; SLC4A1AP; DDX49; POP4; RTCA; ZC3H3; CELF3; RTCB; BCCIP; IFIT5; MKI67; PHF6; IFIT3; ALKBH8; MRPL41; MRPL4; IFIH1; PNN; HMGN5; SART3; SNRNP70; ALKBH1; CWC22; RPL36; HIST1H1B; MRPS27; CLUH; EIF1AX; PRMT1; DDX11; DARS2; DDX51; DNM1; FTSJ3; SARS2; NOA1; RBM12B; TUT1; SRFBP1; NSRP1; STAU2; DDX1; CSTF2; SLC3A2; MRPS30; C1ORF52; JAKMIP1; HTATSF1; HSD17B10; HSP90B1; RPF1; HSPD1; DHX30; STIP1; POLR2B; PES1; KIAA1324; DNAJC21; RRS1; SURF6; POLR2G; ZNF622; ASCC3; APOBEC3D; FDPS; NOP58; CHTOP; CPSF7; COA1; PNO1; MCRS1; SAMD4A; CDC5L; PA2G4; SRP68; EIF2S1; TARBP2; PARP12; MANF; RPS26; MEX3B; HIST1H4A; PIN4; KIAA0907; SLIRP; RSL24D1; DZIP3; RAN; TNRC6A; TPT1

Go Cellular

	Term	*% Count*	*P-value*	*Combined Score*	*Genes*
1	primary lysosome (GO:0005766)	30%	0.007798	33.51317	DEFA4; AZU1; MPO
2	mRNA cleavage and polyadenylation specificity factor complex (GO:0005847)	24%	0.005353	28.3221	CPSF7; ZC3H3; CSTF2; TUT1
3	preribosome, large subunit precursor (GO:0030687)	23%	0.000721	38.42503	PES1; RRS1; ZNF622; AAMP; RPF1; FTSJ3
4	nuclear chromosome (GO:0000228)	19%	6.85E-05	42.44075	TOP2A; HIST1H4A; RAD50; HIST1H3A; RRS1; RCC1; BIRC5; HMGA2; TUBG1; SMC2
5	intrinsic component of mitochondrial inner membrane (GO:0031304)	17%	0.007628	19.34808	COA1; COX16; PET100; TIMM17B; COX11
6	preribosome (GO:0030684)	12%	0.0051	14.57805	LTV1; NOP58; PES1; RRS1; SRFBP1; ZNF622; AAMP; FTSJ3; RPF1
7	centriole (GO:0005814)	11%	0.008209	11.63477	TOP2A; IFT88; BCCIP; DZIP1L; CNTROB; DZIP1; CEP290; TOPORS; RAN; CEP128
8	microtubule organizing center part (GO:0044450)	10%	0.003322	13.55194	TOP2A; BCCIP; TOPORS; CEP128; IFT88; TNKS2; LCK; DZIP1L; CNTROB; DZIP1; CEP290; RAN; CDK5RAP2
9	mitochondrial matrix (GO:0005759)	8%	0.004311	9.767557	ISCA2; PAM16; BCKDHB; DARS2; PDHB; ATP5F1; HSD17B10; ACSF2; COQ5; HSPD1; SARS2; OXCT1; ETHE1; ATP5E; IDH3B; PDK3; PDSS2; PDSS1; ACADM; NAGS; MRRF; MTRF1L; PDK1; BCAT2
10	nucleolus (GO:0005730)	7%	0.005099	7.90751	ZNF771; TOP2A; DDX49; DDX1; DCTN3; XPC; SDAD1; MKI67; PHF6; SMC2; RPF1; PES1; SNAPC3; RPL36; RRS1; TRIM68; PDK3; SURF6; ZNF622; ZNF146; N4BP1; PDK1; DFFB; NOP58; CBX5; PNO1; DDX11; MCRS1; SETMAR; DDX51; PA2G4; SIRT7; MIF4GD; FTSJ3; UBLCP1; FANCD2; TMEM217; TUT1; PIN4; CIAPIN1; RSL24D1; ATF3; SPC24; RAN

KEGG PATHWAYS

	Term	*% Count*	*P-value*	*Combined Score*	*Genes*
1	Non-homologous end-joining	23%	0.016864	21.68306	RAD50; DCLRE1C; POLM
2	Nucleotide excision repair	13%	0.015554	12.23248	POLE4; RFC3; ERCC3; POLD1; XPA; XPC
3	Glutathione metabolism	13%	0.010372	13.14335	RRM1; RRM2; GSTO2; GPX3; GPX7; TXNDC12; GGT1
4	Transcriptional misregulation in cancer	10%	0.000492	17.90869	ZBTB17; CDKN1B; HIST1H3J; HMGA2; IGH; MPO; FOXO1; CDK9; HHEX; HIST1H3A; DDIT3; ID2; REL; ITGB7; HIST2H3D; HIST1H3B; FCGR1A; HIST1H3C; BIRC3
5	Protein processing in endoplasmic reticulum	8%	0.012998	8.480882	SEC24B; UBE2D4; CUL1; UBE2D1; EIF2S1; HSP90B1; MAPK9; HSPH1; BAG2; DDIT3; STT3A; UGGT2; SEC24D; TXNDC5
6	AMPK signaling pathway	7%	0.02096	2.895559	CRTC2; CREB1; RPS6KB1; CREB3L2; RPS6KB2; PIK3CD; ADIPOR2; FOXO1
7	Cell cycle	6%	0.01555	2.614352	ZBTB17; GSK3B; CDKN1B; MCM7; ESPL1; ORC2; CUL1; E2F3
8	Oxidative phosphorylation	6%	0.03042	2.083761	PPA1; NDUFA3; ATP6V0A2; COX11; NDUFB1; COX7C; COX6B1; LHPP

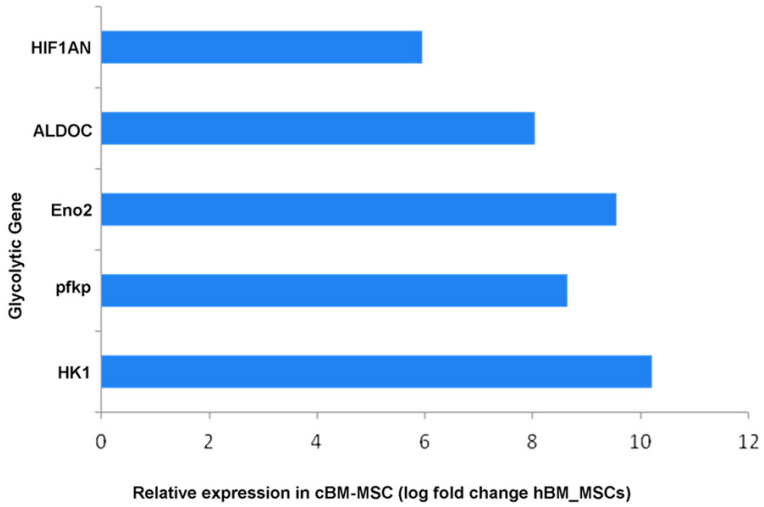

Figure S2. Bar-graph showing relative expression of glycolytic genes in cBM-MSCs (log fold change) with respect to healthy BM-MSCs.

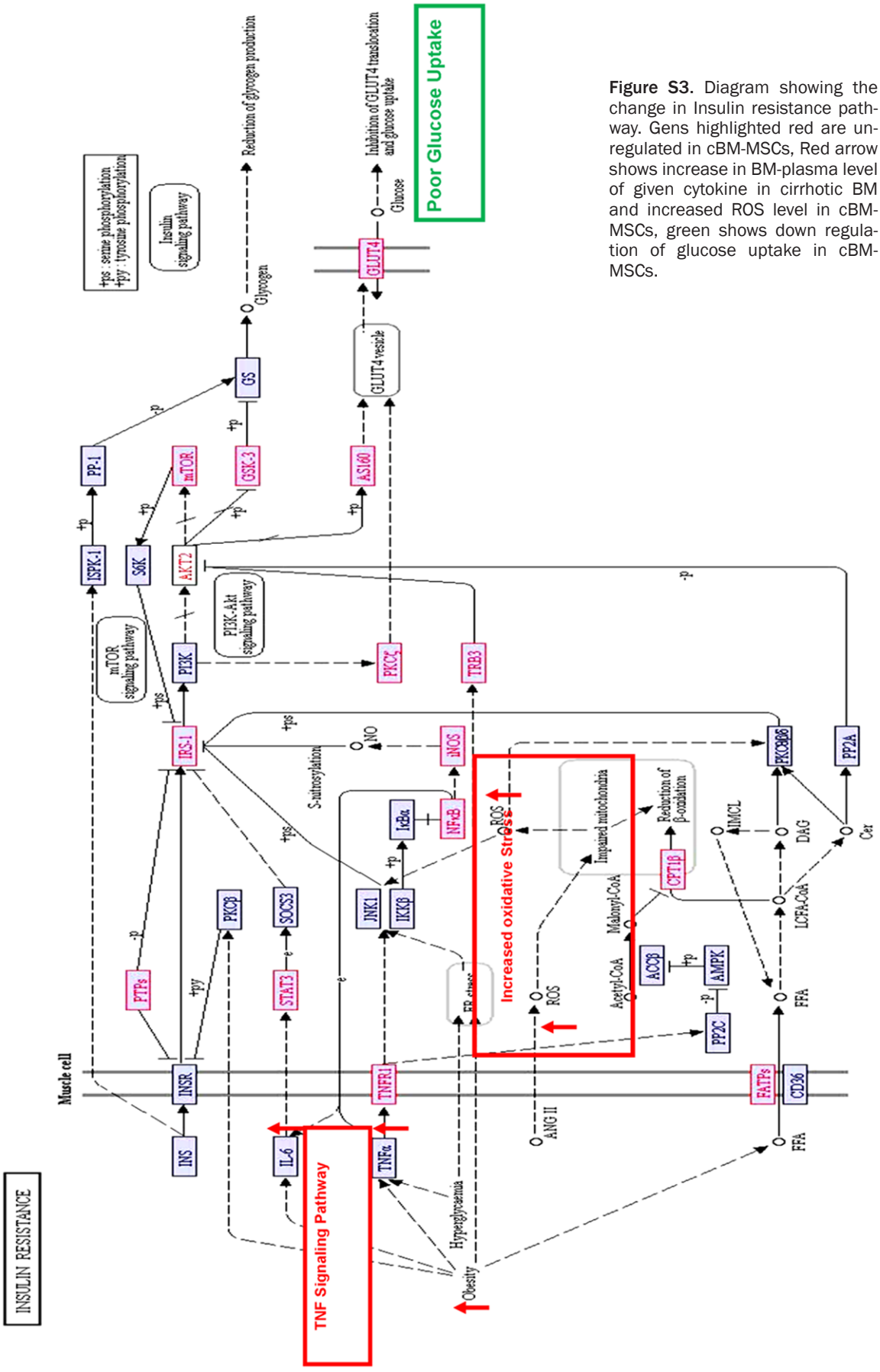

Figure S3. Diagram showing the change in Insulin resistance pathway. Gens highlighted red are unregulated in cBM-MSCs, Red arrow shows increase in BM-plasma level of given cytokine in cirrhotic BM and increased ROS level in cBM-MSCs, green shows down regulation of glucose uptake in cBM-MSCs.

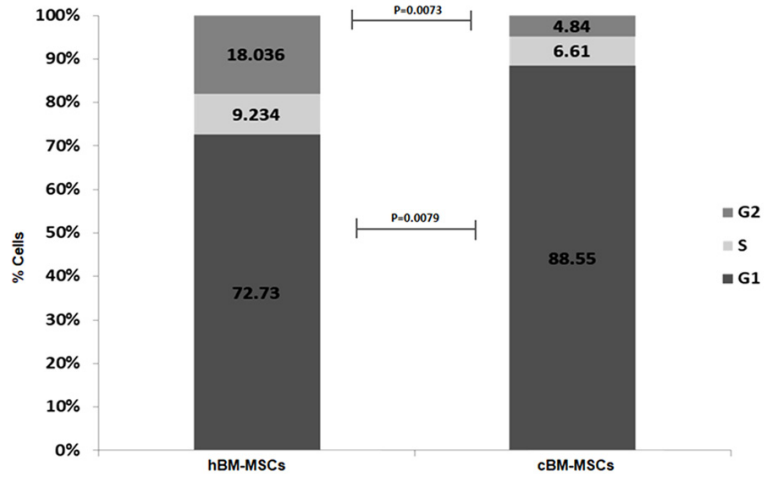

Figure S4. Bar graph showing average present of cells present at different stage of cell cycle of passage 5 hBM-MSCs and cBM-MSCs.